FUNCTIONAL MATERIALS FOR FUNDAMENTAL RESEARCH AND APPLIED SCIENCE: SYNTHESIS AND CHARACTERIZATION

SYNOPSIS

OF THE Ph.D. THESIS SUBMITTED

TO

MANGALORE UNIVERSITY

FOR THE AWARD OF DEGREE OF

DOCTOR OF PHILOSOPHY

in

CHEMISTRY

By

Mr. Sachin Ashok Bhat

Reg. No: MU/EXB/Ph.D./CR.212/Chem./2018-2019/E-13

Centre for Nano and Soft Matter Sciences
Bangalore - 562 162, INDIA

July – 2021

Name of the Ph.D. candidate : Mr. Sachin Ashok Bhat
Senior Research Fellow

Work place: Centre for Nano and Soft Matter Sciences
Arkavathi Campus, Survey No.7,
Shivanapura, Dasanapura Hobli,
Bengaluru – 562162

Title of the Thesis: "Functional Materials for Fundamental Research and Applied Science: Synthesis and Characterization"

Date of registration: 01-03-2017

Registration No. No. MU/EXB/Ph.D./CR.212/Chem./2018-2019/E-13
Intimation letter dated 26.02.2019

Name of the research supervisor: Dr. C. V. Yelamaggad
Centre for Nano and Soft Matter Sciences
Arkavathi Campus, Survey No.7,
Shivanapura, Dasanapura Hobli,
Bengaluru - 562162

Preface

Functional materials, being truly exceptional chemical substances primarily built from diverse organic and/or inorganic fragments, exhibit predestined characteristic functions/phenomenon/properties that have promising significance in a wide range of modern practical applications as well as in fundamental research.[1] Currently, they have been attracting a great deal of attention not only because they can serve as the novel media for a large variety of devices (appliances) but also assist significantly in developing innovative technological concepts. Such materials include nanoparticles, [2] metallic oxides, [3] metal-ligand coordination polymers (COPs), [4] metal-organic frameworks (MOFs), [5] covalent organic frameworks (COFs), [6] thermotropic liquid crystals (mesogens), [7] metallomesogens, [8] liquid crystal-nanoparticle (LC-NP) hybrids, [9] organic-inorganic hybrid semiconductors, [10] conducting polymers, [11] carbon nanotubes, [12] graphene [13] etc. These materials have been proven to be extremely promising in the arenas of display technology, chemical sensing, photonics, fluorescence, biomedicine/healthcare, actuation, electronics, magnetism, energy conversion & storage, transduction, ferroics, piezo- and pyroelectrics, superconductors, automotive industries etc. [2-13]

Most importantly, functional materials can transform one form of energy into another. For example, mechanical energy can be converted into electrical energy in piezoelectric materials. Thus, functional materials constitute an important class of materials facilitating cutting-edge fundamental research and technology developments leading to applications in different areas. However, to widen their usage in unexplored and intersectoral regions, there is a need for rational design insights and innovative synthetic methodologies in realizing new functional materials featuring a broad spectrum of desired physical properties. In this thesis, we describe the molecular design, synthesis, and characterization as well as some intrinsic functional properties of three different classes of novel materials namely, (i) thermotropic liquid crystals (LCs), (ii) liquid crystal-nanoparticle (LC-NP) hybrids, and (iii) coordination polymers (COPs)

I. Liquid crystals

Liquid crystals (LCs) are a distinct phase of matter whose structural order is intermediate between conventional liquids and solids. They have attracted considerable attention because they form the basis of every living being and serve as active media in technological applications. They show a range of unique properties that are promising from the viewpoints of both fundamental research and applied science. [7]

I.1. Classification of liquid crystals

Depending upon how the LC phases are attained or formed, they have been classified into lyotropic and thermotropic. The action of solvent (mostly water) on amphiphiles yields lyotropics, whereas the influence of heat on LC molecules/amphiphiles (mesogens) furnishes thermotropic LCs. Thermodynamically stable mesophases appearing during both heating and cooling cycles are termed *enantiotropic*, while the LC phases formed only during the cooling cycle are *monotropic.*

I.1A. Lyotropic liquid crystal

Lyotropic LC phases, also referred to as lyomesophases, are generally realized by mixing amphiphilic molecules with the solvents (usually water) at a given temperature in a specific ratio. Lyotropic LCs vary in their structures that largely depend upon the temperature, the nature of the constituent polar organic molecules (amphiphiles), and the amphiphile/solvent (water) ratio. However, the work presented in this thesis focuses on thermotropic LCs exclusively.

I.1B. Thermotropic liquid crystals

Liquid crystalline materials are referred to as thermotropic if they display phase transitions due to temperature changes. Generally, they are shape-anisotopic organic or metal-containing organic molecules (mesogens), and their self-assembly, caused due to the action of heat, yields thermotropic LC phases. Upon heating mesogen, at a given melting temperature, the solids sharply transform into LC (anisotropic) phase wherein, along with the molecular mobility, long-range order exists in at least orientation of mesogens. Upon further heating, at a given clearing (high) temperature, the long molecular axes of the mesogens randomly orient due to loss of the orientational order, resulting in the liquid (isotropic) phase. Indeed, on cooling from the isotropic state, these phase transitions can be reversed. The mesogens may show a series of LC phases essentially differing in their structural symmetries. Here, the disappearance in one, two, or three dimensions of long-range translation periodicity in the crystal may precede the long-range orientational order collapse.

I.1.1. Classification of thermotropic liquid crystals

I.1.1A Conventional liquid crystals

Generally, thermotropic conventional LCs are constituted by shape-anisotropic molecules (mesogens), which are either rod-like[7a] or disc-shaped.[14] Using these classical rod-like (calamitic) and disc-shaped (discotic) mesogenic cores, various monomers,[7a,c,d] oligomers [7e] and polymers [7g,] exhibiting thermotropic mesomorphism have been realized, and their properties have been investigated. [7,8] The incorporation of molecular chirality in the molecular architecture of

such materials has yielded chiral mesogens that are known to display helical (chiral) superstructures and the frustrated LC phases. [15]

I.1.1B. Nonconventional liquid crystals

There is yet another vital class of thermotropic LCs, called nonconventional LCs, where the constituent mesogens' anisotropic shape deviates significantly from conventional LCs. [16] It has been well demonstrated over the years that the mesogens with such unconventional molecular structures also display liquid crystallinity. The combination of incompatible molecular fragments such as flexible units (tails and spacers) and rigid (anisometric) cores(s) is such that the resultant molecular architecture does not resemble classical structural design. Notably, they display complex/intriguing mesophases besides conventional LC phases. Examples of nonconventional LCs include polyhydroxy amphiphiles, [16] taper shaped molecules, [16] rod-coil molecules [16] oligoamides, [16] polycatenars, [17] bent-core (banana-shaped &V-shaped) LCs. [18] and oligomers (dimers, trimers, tetramers, etc.) [19] and soft-nano composites. [20,21]

I.2. Liquid crystal-nanoparticle (LC-NP) hybrids

As discussed earlier, LCs represent an exciting class of soft-matter, while remaining in a fluid state, possess intrinsic long-range order and thus, they exhibit a range of exceptional properties which are not only fascinating from a basic research point of view but also hold huge potential for a wide variety of advanced technological applications. [7] Nanoparticles (NPs), being ultrafine particles with a diameter size less than 100 nm, show a range of remarkable optical, electronic, magnetic, and chemical properties. [2,3] Even though NPs are known to be associated with modern science, they have a very long history. For the first time, the NPs synthesis was introduced by Michael Faraday in his legendary paper in 1857 [22l,] which describes the optical properties of nanoscale metallic particles. Some of the exciting properties of the nanoparticle are highlighted below.

I.2A. Physical properties: All the NPs, irrespective of their chemical nature, possess large surface area, and thus, their physical properties such as stability and solubility are influenced mainly by the nature of their surface [2]

I.2B. Optical Properties: They absorb and scatter the light with very high efficiency. Ranging from vibrant reds to blues, colloidal gold can exhibit a wide range of colors, depending on the particle size, shape, local refractive index surrounding the particle, and aggregation state. These colors arise due to a phenomenon known as Localized Surface Plasmon Resonance (LSPR), where conduction electrons on the surface of the nanoparticle oscillate in resonance with incident light.[3]

I.2C. Other size-dependent properties: These include chemical reactivity, SPR, electrical conductivity, fluorescence, magnetic permeability, tunneling (quantum effect) etc. [2]

Hence NPs, especially Gold NPs (AuNPs), are finding their uses in various arena such as diagnostics, separations, sensing, catalysis etc.[22] In recent years, there have been constant efforts in developing an altogether different class of hybrid materials where the LC and NP concepts have been combined by realizing their hybrid motifs. [20] As mentioned earlier, due to their strong optical resonance, arising from localized surface plasmon, metal nanoparticles (MNPs) find a wide range of applications in various devices such as photonics, sensors, photovoltaics etc. The properties of SPR can be modulated effectively by changing the nature of NPs; for example, by associating NPs with LCs, anisotropic NPs featuring dielectric behaviour can be realized. [20] Currently, such LC-NP hybrids/composites are of great interest because they can exhibit remarkable optical properties such as negative refraction and hyperlensing – the essential characteristic features of metamaterials.[20] Currently, a wide variety of 2D and 3D structures made of spherical AuNPs have been obtained by decorating NP surfaces with mesogenic or promesogenic molecules. [21] Thus, the NPs with mesogenic coating can be considered as potential candidates for various applications.[20] Thus, there is a need to prepare LC-NP hybrids to develop 'Smart Functional Materials' for multiple applications. It can be achieved either by physical mixing of NPs with LC phases or by binding/associating mesogens with NPs.

I.3. Coordination polymers (COPs)

In recent times, the metal-ligand coordination polymers [4] and metal-organic frameworks (MOFs) [5] have been the subject of sustainable interest for chemists, biologists, physicists, and material scientist because of their vast promise for applications in gas storage, chemical sensing and separation, heterogeneous catalysis, membrane and electronic devices, magnetism, etc. COPs have been mostly regarded as next-generation, feasible functional materials as they can be readily realized with choice of the structural-dimensionality through "bottom-up" synthetic approach that primarily involves the appropriate selection of coordination geometry of metal ion center and guest ligands.[5a-f] Their infinite structures with repeating coordination segments in one-, two- and three-dimensions manifest in the form of versatile arrays such as long chains, sheets, and 3D networks.[5a-k] Moreover, such hierarchy structured arrays, depending upon constituent inorganic and organic moieties' chemical characteristics, can generate diverse supramolecular motifs resulting from H-bonds, π-stacking, dipole-dipole or van der Waals interactions. In fact, such secondary forces enable COPs to transform their structures reversibly.[5i] COPs, owing to their diverse topological order coupled with coordination geometries, display a wide range of promising phenomenon viz., adsorption/separation,[5f] molecular recognition,[5h], luminescence,[5l-n] thermoelectricity, [5o-q] host-guest behavior,[5s] electrical conductivity [5g, 5j-k,] magnetism [5r-t] etc.

I.3.1. Classification of COPs

There are several ways to classify COPs that are based on their structure and composition. One of the most general classification methods is by considering the macroscopic dimensions of the COPs. Specifically, they are categorized as one dimensional (1D), two dimensional (2D) and three dimensional (3D). In 1D COPs, the structure extends in a straight line, along the x axis, whereas in the 2D COPs, the network extends in a plane (two directions x & y axes). The structure extends in all three directions (x, y, & z axes) in the 3D COPs.

Scope and outlook of the thesis

As previously mentioned, functional materials include various classes of technologically relevant synthetic materials that are by and large are organic or inorganic substances or organic-inorganic hybrids or composites ranging from low molar mass compounds to polymers. However, this research area has a vast scope where new functional materials can be designed, synthesized, and characterized. This reasoning formed the basis of the work carried out and embodied in the present thesis covering three essential classes of functional materials viz., Liquid Crystal Dimers, Liquid Crystal-Nanoparticle Composites, and Coordination Polymers.

Liquid crystal dimers made by covalently tethering two mesogens via a flexible spacer have been in the limelight due to their ability to act as model systems for LC polymers, and they display unusual thermal properties which differ from that of the conventional monomeric LCs [19]. One of the most important characteristics is their phase transitional behavior depends mainly on the length and parity of the spacer connecting the two mesogenic segments, which is popularly known as the odd-even effect. Such a result has been interpreted in terms of the overall molecular shape of dimers in their all-*trans* conformation, which is primarily dictated by the spacer's parity. A dimer with an even-parity spacer attains nearly a linear shape, whereas an odd-membered dimer gains a bent-shape wherein the mesogenic cores are inclined to one another. The LC dimers are broadly divided into two categories: (a) symmetric dimers - comprise two chemically identical mesogenic cores, and (b) nonsymmetric dimers – comprise two non-identical LC cores. While the symmetric dimers have been regarded as model motifs for LC polymers, the nonsymmetric dimers have gained importance owing to their rich phase transitional behavior. The LC properties of nonsymmetric dimers depend on, besides the length and parity of the spacer, the chemical nature of the two mesogenic units and their terminal substituents. In particular, the nonsymmetric, optically active (chiral) dimers derived from, naturally occurring cholesterol have been attracting a great deal of attention because they exhibit

unusual phase sequences and stabilize frustrated LC phases and technologically significant LC phase over the wide thermal range.[23] Thus, we have designed, prepared, and characterized three series of nonsymmetric dimers where three different mesogens, comprising two or three benzene rings, been covalently linked with cholesterol through the ω-oxyalkanoyloxy flexible spacer of varying length and parity.

LC-NP composites made either by coating NPs with LC ligands or by adding small quantities of NPs with the host LCs are drawing researchers' attention because of their ability to display a wide range of properties with improved characteristics. The former composites are especially impressive as they, being single –component systems, show the signatures of both LCs and NPs. Moreover, by using appropriate LC segments for coating the central MNP scaffold, it is possible to dictate or drive the self-assembly of NPs into hierarchical structures having relevance in both fundamental research and practical applications. Such composites show anisotropic properties [21m] / SPR variation of the NPs [20j, 21m & 21n], electromechanical memory effect in isotropic phase [21], the ability to stabilize & widening the thermal range of blue phases (BPs) [21o], the capability of enhancing the conductivity of columnar LCs – organic photovoltaics [21n], the capacity of enhancing the electro-clinic effect of chiral SmA phase [21] etc. Hitherto, mesogens such as calamitics, discotics, and bent-core LCs have been used as capping ligands to NPs to study the self-assembly properties of the LC-NP composites formed. Seemingly, the nonconventional LCs have not been explored for the preparation of LC-NP composites. Inspired by these observations, we intended to insert the nonconventional mesogens viz., dimer-like core and dimeric entity, in the molecular design of LC-NP composite. Thus, we have synthesized and characterized three series of single-component LC-NP composites where gold (Au) NPs (AuNPs) have been capped with mesogenic primary amines.

As previously noted, the COPs, formed by the reaction between metal ions and the organic ligands, have been recognized as vital classes of functional materials because they display a wide variety of properties having great potential in a broad range of applications. Their structural diversity and functionalities can be not only modulated by the selection of metal ions and the bridging ligands but also through secondary (weak) interactions such as π-π stacking, van der Walls associations, H-bonds etc. Apparently, the COPs derived from the supramolecular synthons where specific intermolecular interactions occurring *via* H-bonds have been rarely reported. Thus, the rational designing of molecular fragments of COPs, especially organic linkers (ligands), is paramount to realize COPs where H-bonds play a crucial role. Working in this direction, we have synthesized three different types of COPs by varying the ligand and metal ion and probed them for their properties.

In this thesis, entitled **"Functional Materials for Fundamental Research and Applied Science: Synthesis and Characterization,"** the synthesis and characterization of novel

compounds belonging to three major classes of functional materials have been presented. The thesis has been divided into four Chapters (**I-IV**), which are further subdivided into sections depending upon the need. The first Chapter focuses on the fundamental aspects, classification, and applications of functional materials. Chapters II, III, and IV illustrate the work carried out during the doctoral study. These chapters begin with a relevant preamble of the topic, followed by the work description, and end with the appropriate references.

General remarks

The molecular structures of all the target compounds have been established indubitably with the aid of standard spectroscopic (UV-Vis, FTIR, ^{1}H NMR, ^{13}C NMR, XRD, XPS, EDAX and Mass) data as well as elemental analyses. The morphology and size distribution have been analyzed with the help of standard electron microscopic techniques such as Field Emission Scanning Electron Microscope (FESEM) and High-Resolution Transmission Electron Microscopy (HRTEM). Since most of the intermediates synthesized are reported compounds, they have been characterized with FTIR and ^{1}H NMR data only. The phase transition behavior of the target mesogens has been evaluated with the help of polarizing optical microscopy (POM) and differential scanning calorimetry (DSC). X-ray powder diffraction (XRD) study has been carried out on certain representative materials. TGA studies have been carried out to analyze the thermal stability of the compounds. The emission property of the compounds has been probed using a photoluminescence spectrometer. The electrical, thermoelectrical, and magnetic properties have been characterized with the help of CCR (Close Circuite Refrigerator) and SQUID magnetometer, respectively.

Chapter I: Introduction to functional materials and applications

Chapter I is an introductory section wherein a brief preamble to some of the fundamental aspects and descriptions of functional materials and their essential properties are presented. This Chapter essentially helps the readers understand the significance of the research work carried out, which has been shown in other Chapters (III to IV) of the thesis. In particular, it deals with the definition and properties of functional materials belonging to three principal categories. In the concluding section, important applications of all such functional materials have been presented briefly.

Chapter II: Molecular Design, Synthesis and Characterization of Nonsymmetric Liquid crystals Dimers Derived from Cholesterol

This Chapter describes the rational design, synthesis, and characterization of three series (II.1, II.2 & II.3) of new cholesterol-based LC dimers. They have been designed to exhibit

technologically important phases such as chiral nematic (N*) and chiral smectic C (SmC*) phases. It is known that when such attempts are made, the frustrated LC phases viz., blue phases (BPs), and/or twist grain boundary (TGB) phase, and/or the smectic A (SmA) may also accompany the aforesaid important mesophases. [19e] The N* and SmC* phases, possessing helical superstructure (handedness), have been respectively employed in temperature-sensing devices and LC displays (LCDs), respectively. [15] Three blue phases, BP-I, BP-II, and BP-III, occur over a short temperature range between the thermal width of helical and isotropic (I) phases of highly chiral mesogens. They reflect visible light of a particular wavelength, and thus, they can be used in color displays, light filters, lasers etc. [15a]. Three TGB phases exist at the phase transition from the I/N* to SmA/SmC* phases over a narrow temperature interval. They have been abbreviated as TGBA, TGBC, and TGBC* phases wherein the layered structure is of the orthogonal SmA, tilted SmC, and helical SmC* phases, respectively. The SmA phase of chiral mesogens has also gained importance in applied science. It is potentially promising as it displays the electroclinic effect - a novel phenomenon used in spatial light modulators. [15a]

Three series (II.1, II.2 & II.3) of nonsymmetric dimers have been realized by covalently linking cholesterol with three dissimilar rod-like cores through an ω-oxyalkanoyloxy spacer. The first series is made by connecting a cholesterol unit to the terminal position of a three-ring calamitic core, namely, phenyl 4-(benzoyloxy)benzoate via a flexible spacer of varying length and parity. The terminal tail length attached to the three-ring core has also been varied to divulge the structure-property-correlations. The dimers belonging to the second series comprise cholesterol and phenyl 3-phenylpropiolate (two-ring) segments interlinked through various ω-oxyalkanoyloxy spacers. The two-ring core has been substituted with long tails of different lengths. The third series possesses two sets (subseries) of dimers where the cholesterol is interlinked with two other two-ring mesogens, namely, Schiff base or salicylaldimine cores. The terminus of both two-ring cores is substituted with chiral tails such as (*R*)- or (*S*)-citronellyloxy and (*R*)- or (*S*)-octan-2-yloxy chains.

II.1. **Nonsymmetric dimers comprising cholesterol and two or three-ring calamitic core**

This section presents a brief overview of cholesterol-based nonsymmetric dimers. Fundamentally, it describes the relationship between molecular structure and mesomorphism of optically active dimers derived from cholesterol. As discussed earlier, the cholesterol-based nonsymmetric dimers have secured a particular position in the field of soft matter. They exhibit exceptional phase sequences, highly frustrated fluid structures, reentrant phases etc. They also offer strategies for modulating the parameters of technologically relevant LC phases.[23] In addition to cholesterol, the chemical nature of the mesogenic (non-cholesterol) entities as well as the length and parity of the spacer, play a vital role in determining their features, such as described above. The non-cholesterol entities generally used are two- or three-ring mesogens.

The examples include Schiff base, salicylaldimine, azobenzene, tolane, chalcone, stilbene, banana-shaped bent-core, phenyl benzoate, terphenyl, biphenyl, diphenyl butadiene, supramolecular motif, etc.[23] The mesogenic core terminus possess substituents such as cyano, nitro, alkyl, alkoxy, alkyl ester, perfluoroalkoxy groups, etc. The lateral substituents such as nitrile, nitro, halo atom(s) have also been incorporated into dimers' structure. A range of spacers such as ω-oxyalkanoyloxy (ester), oxyalkoxy (ether), alkanedioic, diynedioic, and oxyalkoxycarbonyloxy (carbonate) moieties have been used to join cholesterol covalently with aforesaid conventional mesogenic cores. Thus, we intended and realized optically active (chiral) dimers where cholesterol is linked to either a two-ring or a three-ring mesogenic core through a ω-oxyalkanoyloxy of varying length and parity.

II.2. Nonsymmetric dimers comprising cholesterol and phenyl 4-(benzoyloxy)benzoate (three-ring) segments.

This section deals with the synthesis, molecular structural characterization, and liquid crystal behavior of sixteen new nonsymmetric dimers (Series II.1) formed by covalently connecting a three-ring mesogen to a cholesterol unit via an ω-oxyalkanoyloxy spacer. We have been working in this research area rigorously for a long time to understand the correlation between the molecular structure and phase transitional behavior and realize technologically significant mesophases over a wide thermal range covering room temperature. To continue our research work in this fruitful area, we intended to design and prepare new cholesterol-based dimers and characterize them. We mainly chose to work on dimers capable of stabilizing technologically related mesophases such as the N* and SmC* phases occurring over a wide thermal range, possibly covering the room temperature. The literature survey shows that three-ring mesogenic cores favor such mesophases. [19] Accordingly, we have prepared and evaluated the LC property of a new set of optically active, nonsymmetric dimers (Series II.1) where the pro-mesogenic cholesterol has been linked to a phenyl 4-(benzoyloxy)benzoate (three-ring) core through an ω-oxyalkanoyloxy spacer. In particular, four sub-series of dimers have been realized by employing three even-membered spacers, namely 4-oxybutanoyloxy (C_4), 6-oxyhexanoyloxy (C_6) and 8-oxyoctanoyloxy (C_8), and an odd-parity spacer viz., 5-oxypentanoyloxy (C_5). In each series, the three-ring core is terminally substituted with *n*-hexyloxy, *n*-decyloxy, *n*-dodecyloxy, and n-tetradecyloxy tails. The general molecular structure of these new sixteen dimers synthesized is shown below. The acronym **CPD-*n,m*** has been used to describe this series of dimers. Here, **C, P,** and **D** respectively signify cholesterol, phenyl 4-(benzoyloxy)benzoate, and dimer. The abbreviations ***n*** and ***m*** respectively refer to the number of carbon atoms in the terminal alkyl chain and the number of methylene units in the spacer.

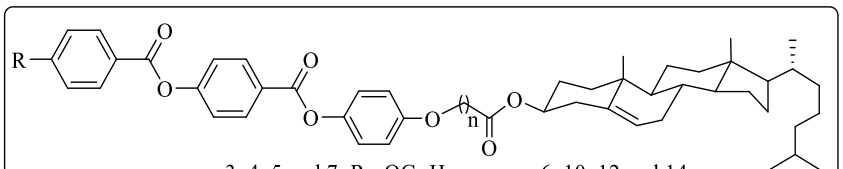

n = 3, 4, 5 and 7; R= OC_mH_{2m+1}; m = 6, 10, 12 and 14

Series-II.1 (CPD-*n*,*m* Series)

These dimers belonging to Series-II.1 (**CPD-*n,m*** Series) have been synthesized following an appropriate synthetic scheme. The thermal behavior of the dimers was probed with different techniques such as POM, DSC and XRD. They exhibit enantiotropic N* and SmC* phases. Some of the dimers also display frustrated mesophases such as BP and TGBC* phases. The dimers possessing an odd-parity spacer stabilized the BP over a thermal range of 0.8º – 0.9º, which agrees with the general observation that odd-membered chiral dimers display BPs due to their bent conformation. Notably, in some cases, the N* and SmC* phases persist over the thermal width of 33-119º and 62-121º, respectively. The members with higher chain lengths showed the TGBC* phase over a wide thermal width of 90º-128º along with the N* phase. The photophysical properties have been ascertained by measuring the UV-Vis absorption spectra of the dimeric compounds. The chiroptical behavior was examined by the circular dichroism (CD) spectroscopic method. The CD technique revealed the N* phase's twist-sense, which is known to be possessing macroscopic handedness.

II.3: Nonsymmetric dimers consisting of cholesterol and phenyl 3-phenylpropiolate (two-ring) mesogenic entities.

This portion of the Chapter describes the preparation, molecular structural characterization, and thermal behavior of sixteen new chiral dimeric LCs belonging to Series-II.2. They comprise cholesterol and phenyl 3-phenylpropiolate (two-ring) segments interlinked by an ω-oxyalkanoyloxy spacer of varying length and parity. Such a two-ring core was specially chosen due to its versatility and ability to stabilize the impressive phase sequences. [15b,15c] The terminal chain's length attached to the two-ring mesogen as well as the length and parity of the spacer, have been varied to shed light on the fundamental structure–mesomorphic property relationships. Three even spacers, namely, 4-oxybutanoyloxy (C_4), 6-oxyhexanoyloxy (C_6) and 8-oxyoctanoyloxy (C_8), and an odd-spacer viz., 5-oxypentanoyloxy (C_5) have been employed. Precisely, four sub-series of dimers have been prepared, and in each, the spacer is held constant while the length of the terminal tail has been varied with 12, 14, 16, and 18 carbon atoms. The general molecular structure representing these sixteen new dimers belonging to four subseries is shown below. The mnemonic **CPPD-*n,m*** has been used for ease of presentation. **C, PP**, and **D** respectively refer to cholesterol, phenyl 4-(benzoyloxy)benzoate, dimer, and ***n*** indicating the

number of methylene units in the spacer and ***m*** signifying the number of carbon atoms in each of the terminal tails.

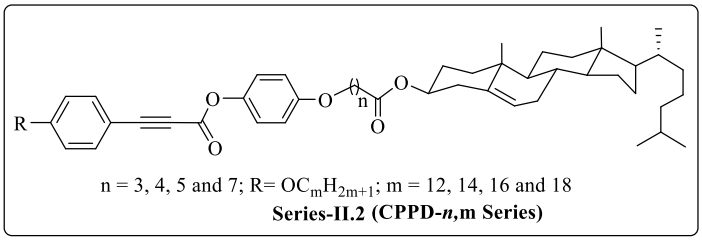

n = 3, 4, 5 and 7; R= OC_mH_{2m+1}; m = 12, 14, 16 and 18

Series-II.2 (CPPD-*n*,m Series)

The characterization results derived from the several complementary techniques reveal that these mesogens, belonging to **CPPD-*m,n*** Series (Series-II.2), display enantiotropic LC phases. In particular, the occurrence of mesophases such as BP-I/II, N*, SmA, and TGBC* phases has been evidenced unequivocally with the help of POM, DSC, and X-ray diffraction. All the four odd-membered dimers commonly exhibit the N* and SmA phases, with a member (**CPPD-5,12**) showing the BP-I/II additionally. The dimers possessing an even-parity spacer display the N* and TGBC* phases. The TGBC* phase exists over the thermal range of 37 °C to 84 °C, which is remarkable because it is a highly complex structure. In a given sub-series, the TGBC* phase's thermal range appears to widen with the terminal tail length increase. Within a series, the clearing (isotropization) temperature generally decreases with the terminal tail length increase. The odd-members possess higher clearing temperatures than those of odd-membered counterparts, as expected. Thus, the phase transitional behavior of these dimers depends on the spacer's parity, called the odd-even effect. The helical twist sense of the N* phase has been figured out with the help of circular dichroism study.

II.4: Nonsymmetric dimers comprising cholesterol and two-ring mesogens derived from Schiff base and Salicylaldamine cores

The synthesis and mesomorphism of thirty-two new stereoisomers in the form of sixteen enantiomeric pairs of cholesterol-based dimers possessing either Schiff base or salicylaldimine mesogenic cores, each terminated with (*R*)- and (*S*)-citronellyloxy or (*R*)- and (*S*)-octan-2-yloxy chains are presented in this section. The two-ring Schiff base and salicylaldimine cores were opted based on the experimental demonstrations that their presence in the molecular design dramatically influences cholesterol-based dimers' LC property. They enable the cholesterol-based dimers to exhibit unusual frustrated LC phases and phase sequences. [19e, 19f] Likewise, chiral tails' insertion in the LC molecular design allows the dimers to show interesting thermal properties.[19j] Thus, in the present molecular invention of cholesterol-based dimers, Schiff base and salicylaldimine cores and chiral tails have been incorporated. Three even-membered spacers, 4-oxybutanoyloxy, 6-oxyhexanoyloxy, and 8-oxyoctanoyloxy, and an odd-parity spacer, 5-oxypentanoyloxy, have been employed to connect cholesterol and two-ring aromatic cores. In

all, four subseries of dimers, two series of Schiff bases (eight dimers in each), and two series of salicylaldimines, have been synthesized. Each subseries comprises four pairs of enantiomers (eight stereoisomers), four (*R*)- & four (*S*)-enantiomers, derived from the combination of four different spacers and a pair of enantiomeric chiral tails which is either (*R*)- and (*S*)-citronellyloxy or (*R*)- and (*S*)-octan-2-yloxy chains. The general molecular structures of these synthesized compounds is shown below. Two each series of Schiff bases and salicylaldimines have been represented with acronyms **CSBC-(*R*/*S*)*n* & CSBO-(*R*/*S*)*n*** and **CSAC-(*R*/*S*)*n* & CSAO-(*R*/*S*)*n*,** respectively. Short forms **C**, **SB, SA, C & O** respectively mean cholesterol, Schiff base, salicylaldimine, citronellyloxy, and octan-2-yloxy. **(*R*)** & **(*S*)** and *n* represent the absolute configuration of chiral tails and the number of methylene units in the spacer, respectively.

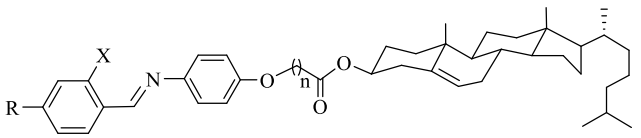

Series-II.3A (**CSBC-(*R*/*S*)*n* Series)**: n = 3, 4, 5 & 7; R = (*R*)- or (*S*)-Citronellyloxy; X= H
Series-II.3B (**CSBO-(*R*/S)*n* Series)**: n = 3, 4, 5 &7; R= (*R*)- or (*S*)-Octan-2-yloxy; X= H
Series-II.3C (**CSAC-(*R*/*S*)*n* Series)**: n = 3, 4, 5 & 7; R= (*R*)- or (*S*)-Citronellyloxy; X= OH
Series-II.3D (**CSAO-(*R*/S)*n* Series)**:: n = 3, 4, 5 &7 ; R= (*R*)- or (*S*)-Octan-2-yloxy; X= OH

All the mesogens realized exhibited enantiotropic LC behavior. Depending upon their structure (the combination of spacer-chiral tail), they display one or multiple mesophases identified as the N*, TGB, SmA, and SmC* phases. Four (*R*)-enantiomers and their (*S*)-counterparts belonging to a series displayed identical phase sequences and phase transition temperatures, as expected. The variation of the chiral tail's nature and the spacers' length and parity appear to affect the dimers' thermal behavior. The Schiff bases/salicylaldimines comprising citronellyloxy tail generally show different thermal behavior than those with an octan-2-yloxy chain. They displayed either the SmA phase's existence or phase sequences such as N*-SmA, SmA-SmC*, TGB-SmA, N*-SmA-SmC* and N*-TGB-SmA-SmC* sequences. The mesophases, namely, the N*, SmA, and SmC* exist in the thermal range of 10-27 ^{o}C, 5.5-150 ^{o}C, and 92- 103 ^{o}C, respectively. Within a series, the clearing temperature decreases with the increase in the spacer length. In all four subseries, the odd-members' clearing temperature was found to be lower than that of the even-parity counterparts, as expected. Interestingly, in some of the dimers, the SmC* phase supercools below the room temperature, i.e., up to -40 ^{o}C. The helical sense (handedness) determination of both the SmC* and N* mesophases was carried out using CD spectroscopic technique. As representative cases, two enantiomeric pairs, one from the Schiff bases and another from the salicylaldimine series, were selected for the CD spectroscopic study. As expected, both the helical phases of an enantiomeric pair displayed the mirror imaging CD bands meaning overall that the chromophores are in the chiral environment. The study also showed that the N* phase's helical handedness is opposite to that of the SmC* phase.

Chapter III: Molecular Design, Synthesis and Characterization of LC-NP Composites

Chapter III deals with the molecular architecting, preparation, and characterization of three series of novel LC-NP composites formed by monolayer coating of central gold (Au) nanoparticles (GNPs) with liquid crystalline dimer-like/dimeric primary (1^o) amines. Here, the 1^o amines possessing the requisite oxidation potential serve as reducing (Au^{3+} to Au^0) agent as well as capping ligands. Most importantly, the introduction of these functionalized (LC) organic ligands on to the central GNP scaffold effectively facilitates the self-assembly of LC-NPs into the LC structure. The first set of LC-NP composites (Series-III.1) has been realized by the monolayer coating the surfaces of GNPs with dimer-like ligands, viz., cholesteryl ω-(4-aminophenoxy)alkanoates. In the second set of LC-NPs (Series-III.2), the GNPs are coated with a monolayer of LC dimeric amines (ligands), namely, cholesteryl ω-((4'-amino-[1,1'-biphenyl]-4-yl)oxy)alkanoates. These dimeric amines (ligands) comprise cholesterol, and 4-aminobiphenyl cores joined covalently via an ω-oxyalkanoyloxy spacer of varying length and parity. The third series of LC-NPs (Series-III.3) includes the novel photoactive soft-nano composite materials. The central GNPs are capped with the LC dimeric amines formed by covalently tethering cholesterol and 4-aminoazobenzene units through a varying ω-oxyalkanoyloxy spacer.

III.1. LC-NP composites: An overview

This section portrays the fundamental aspects of LC-NP composites. It includes a brief discussion about the different synthetic approaches, structural features, mesomorphic behavior, and technological importance of soft-nano (LC-NP) composites.

III.2. LC-NP composites derived from cholesterol-based dimer-like amines

Under this heading, the preparation, molecular structural characterization, and LC behavior of four dimeric amines and the corresponding LC-NP composites are discussed. In recent years, the anisotropic molecular assembly notion into LC phases has been successfully extended to trigger and direct the organization of plasmonic NPs into the functional fluid superstructures. In such structures, some degree of anisotropy and long-range order at the mesoscale level exist. The intrinsic assembling ability of mesogenic (LC) ligands grafted onto the NP surface enables particles to arrange in ordered self-assembled structures that are fluid (mechanically shearable) and respond readily to the external stimuli. Although wide varieties of LC MNPs have been designed and realized, the successful attempts dealing with analogous chiral plasmonic MNPs have been barely reported. In recent pioneering work, it is demonstrated that the organization, size, and morphology of the GNPs can be manipulated effectively by their in-situ preparation using chiral mesophase templates formed by the chiral LC ligands. Notably,

in-situ generated GNPs of the chiral smectic A (SmA*) phase organize in helical fashion while they attain spherical shape and bent conformation in the chiral nematic (N*) and chiral smectic C (SmC*) phases, respectively. However, in the context of the topic described above, there is only one special report where the strong chiral optical response of a mesophase resulting from the spontaneous self-assembly of chiral plasmonic GNPs has been disclosed. These are columnar (Col) arrays (wires) arranged helical manner.[21p] However, for a wide range of technical implications, the organization of plasmonic MNPs in helically twisted LC lamellar (CD active) structure, where the dielectric and conducting regimes are arranged alternatively, as in the case of aforesaid Col phase, is ideal and highly favorable. To our knowledge, such an assembly by LC-NPs has not been accomplished hitherto.

Working in this direction, we have rationally designed and synthesized new chiral LC-NP composites where the GNPs are coated with LC dimeric amines (ligands) derived from cholesterol. This study especially demonstrates that mesogens' molecular chirality could be mapped on to macroscopic structure where helicoidal modulation of the director occurs. The ligands are formed by covalently interlinking cholesterol and 4-aminophenyl mesogenic segments via an ω-oxyalkanoyloxy spacer of varying length and parity. The LC-GNPs preparation methods involve the solution mixing of LC-amines and Au(III) ions at RT either in a glass vessel or on glass plates. The present study's attractive feature is that the rationally chosen LC-amines reduce Au(III) to Au(0) and bind to the central gold scaffold precluding impurities. The chemical structures of LC ligands and corresponding LC-GNPs, ascertained using standard spectroscopic techniques and elemental analysis, have been presented below. For the sake of ease, the acronyms **D*n*-LCL** and **D*n*-LCNPs**, have been used to describe LC ligands and LC-NPs, respectively. The symbols **D**, **L**C, **L**, and **NPs** respectively denote Dimer-like, Liquid Crystal, Ligand, and Nanoparticles; n indicates the number of methylene segments in the spacer.

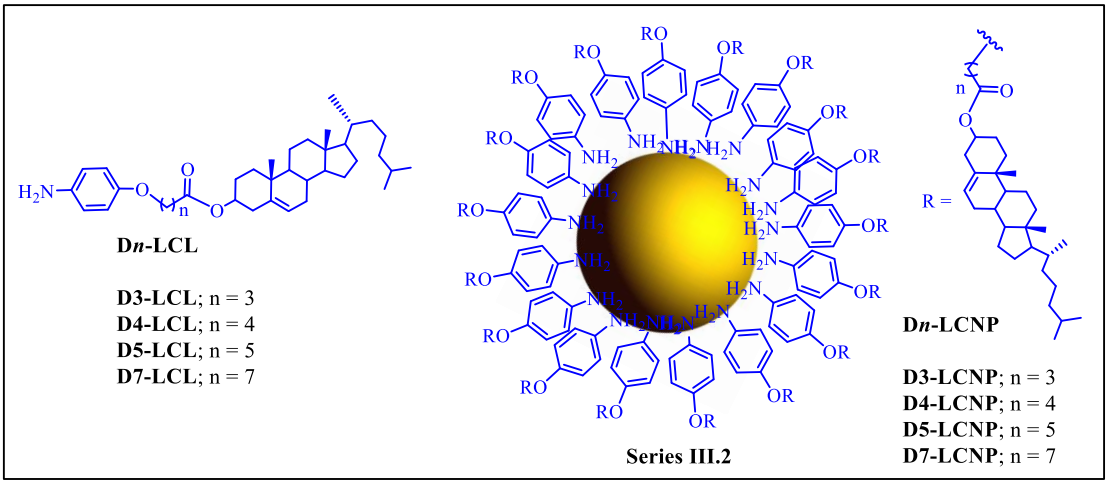

The spectroscopic and elemental analysis results were found to be consistent with the proposed structures of the ligands and LC-NPs. The analysis of HRTEM (high-resolution transmission electron microscopy) images confirmed the spherical shape morphology of the prepared NPs with an average particle size of around 3.3 nm. The UV-Vis spectra show the characteristic absorption band due to surface plasmon resonance (SPR) of the composites. The liquid crystal behavior of both ligands and chiral LC-NP composites was established with the help of microscopic, XRD, and CD techniques. While the ligands exhibit multiple mesophases such as N* TGB, and SmA phases, the LC-NPs display an enantiotropic chiral lamellar (LmX*) phase solely, evidencing the complete formation and monodispersity of the composites. The detailed investigations revealed the self-assembly of chiral plasmonic GNPs into a helically twisted LC lamellar (LmX*) structure where intercalated organization among the LC-NPs occurs. This helical structure shows a chiroptical effect, i.e., the CD activity. In other words, the chiral plasmonic lamellar superstructure results from the directed self-assembly of optically active GNPs. Since the conducting (gold atoms) and dielectric (liquid crystalline organic) regimes have been structured successively in the mesophase, they can serve as a novel media for a wide range of application areas, which would potentially include sensing and catalysis technologies as well as invisibility cloaking devices. Specifically, their interactions with CP light facilitate breaking the degeneracy among two CP waves and enhance the effective refractive index for one polarisation. Therefore, LC-GNPs of the kind presented herein, where the metal volume fractions are generated due to the thick coating of GNPs by optically active LCs, can show a negative refractive index, a crucial phenomenon required for metamaterials.

III.3. LC-NP composites derived from cholesterol-based dimeric amines

This section presents the preparation, structural characterization, and mesomorphism of another set of novel soft-nano (LC-NP) composite materials derived from cholesterol-based dimeric amines. In particular, the four new soft-nano materials have been prepared by grafting liquid crystalline dimeric amines (ligands), namely, cholesteryl ω-((4'-amino-[1,1'-biphenyl]-4-yl)oxy)alkanoates onto the GNP surface. The facile formation of LC-NP materials can be primarily ascribed to the requisite redox property of the amine ligands used. They possess the oxidation potential between the potentials of Au(III) to Au(0) and Au(0) to Au(I) transition. [22k] In this series, the biphenyl core has been incorporated in the molecular skeleton to increase the distance between the peripheral bulky chiral (cholesterol) units and the central GNP, and to make out its effect on the phase transitional properties of LC-NP materials. The molecular structures of the dimeric ligands and the target soft-nano composites realized are shown below. Abbreviations **B*n*-LCL** and **B*n*-LCNPs** have been used to describe LC ligands and LC-NPs, respectively. The alphabet letters/s **B**, **L**C, **L**, and **NPs** stand for Biphenyl-based dimer, Liquid Crystal, Ligand, and Nanoparticles, respectively; ***n*** indicates the number of methylene segments of the spacer.

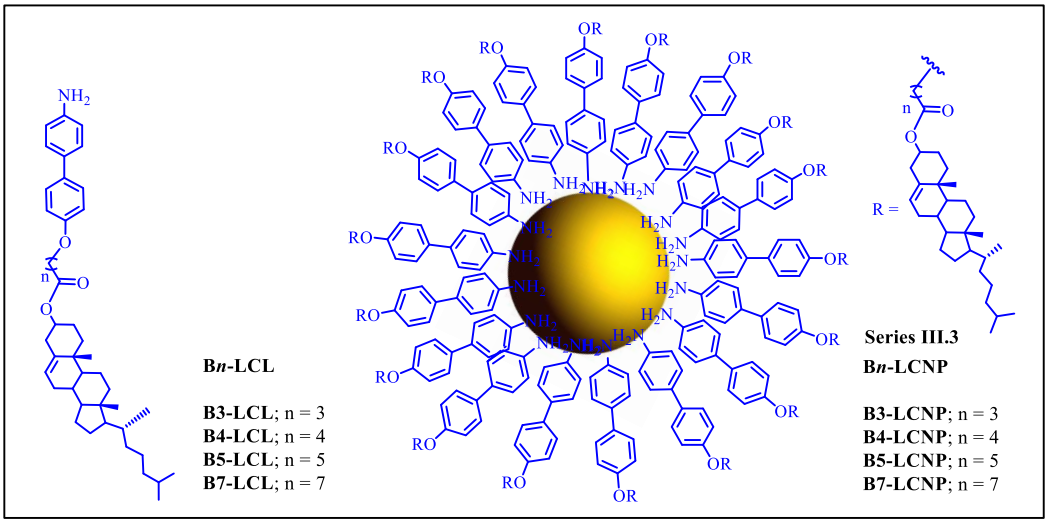

Spectroscopic methods and elemental analysis enabled the unambiguous structural determination of chiral ligand-capped GNPs and their precursors. The NP particle sizes were found to be approximately in the range of 30-40 nm, which are considerably higher than those observed for the soft-nano composites of series III.2, inferring that the LC ligands' structure determines the size of NPs. The LC-NP composites exhibit the typical SPR band in the optical absorption spectra. The ligands display a rich phase behavior stabilizing various mesophases, including BPI/II, N*, TGB, and SmC* phases. Contrary to the ligands' rich mesomorphic behavior, the LC-NPs exhibit an enantiotropic lamellar phase solely, as evidenced by POM, DSC, and XRD studies. The LC phase observed here appears to be identical to that of the LmX* phase of the LC-NPs belonging to Series-III.2. The results of XRD and CD studies, respectively, evidenced the intercalated tilted structure and handedness of the LmX* phase.

III.4. Photoactive LC-NP composites derived from cholesterol-based dimeric amines

The preparation, molecular structural characterization, and phase transitional properties of four new photoactive LC-NPs derived from dimeric amines have been presented in this section. Liquid crystalline dimeric capping agents, namely, cholesteryl ω-(4-((4-aminophenyl)-diazenyl)phenoxy)alkanoates are formed by covalently joining cholesterol and 4-aminoazobenzene entities via an ω-oxyalkanoyloxy spacer of varying length and parity. Thus, the azobenzene unit featuring the *trans-cis-trans* photoisomerization, is expected to render the photo-functional property to the soft-nano composites. The *trans-cis* isomerization occurs when the azobenzene core absorbs the UV radiation of wavelength 365 nm, hence the UV band corresponding to π- π * transition decreases whereas forbidden n-π * peak intensity increases. This can be reversed by shining visible light or by thermal relaxation.[22m] Apart from the shape and size, the dielectric constant of the surrounding environment and the steric factors/repulsions

(or distance) alter NPs' properties. The dielectric constant of the surrounding medium significantly changes the electrons' resonance frequency onto NPs' surface leading to the variations in intensity and wavelength of SPR transitions. [22m-o] To probe the effect of *trans-cis* photoinduced isomerization of azobenzene core on the overall properties of the soft-nano composites comprising plasmonic NPs, the present study was undertaken where four new LC-NPs have been designed incorporating a photoactive segment, synthesized, and characterized systematically. The chemical structures of the azobenzene-based chiral ligands and the target soft-nano composites are shown below. The acronym employed to refer to the ligands and soft-nano materials, respectively, are **A*n*-LCL** and **A*n*-LCNPs.** The alphabet letters/s **A**, **L**C, **L**, and **NPs** stand for Azobenzene-based dimer, Liquid Crystal, Ligand, and Nanoparticles, respectively; ***n*** signifies the number of methylene segments of the spacer.

The structures of the ligands (**A*n*-LCLs)** and LC coated GNPs (**A*n*-LCNPs**) were confirmed using the spectroscopic data and elemental analyses. Investigation of the phase

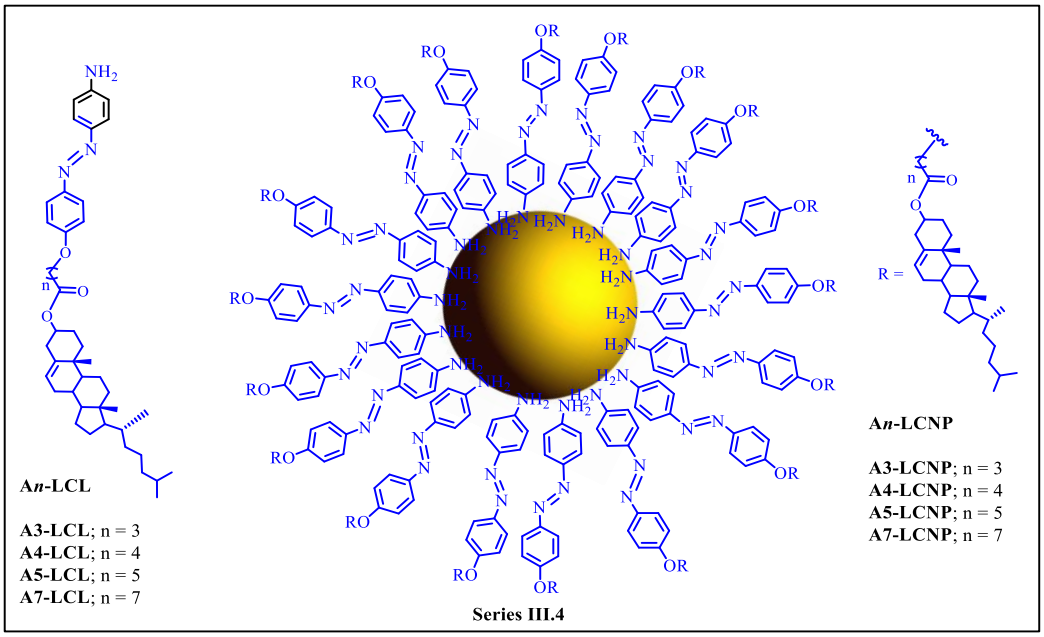

behavior, using several complementary techniques, reveals that the dimeric amines (**A*n*-LCLs)** show LC phases such as N* and TGBC* phases. In contrast, the LC-NPs (**A*n*-LCNPs**) display a thermodynamically stable lamellar phase. XRD and CD studies corroborate that the characteristics of the lamellar phase of the **A*n*-LCNP** materials go well with those of the LC (LmX*) phase exhibited by the soft-nano composites of the Series-II.2 (**D*n*-LCNPs)** and Series-II.3 (**B*n*-LCNPs)**. Notably, the expected variations in SPR peak, i.e., the decreases in peak intensity and redshift in the wavelength, come about after irradiating the micromolar solutions of LC-NPs with 365 nm light for different illumination times. This can be attributed to the drastic change in structure and the dipole moment of azobenzene units of the surrounding medium. That

is, the photoinduced *trans*-*cis* isomerization of the azobenzene units causes such effects. Here, the dipole-dipole interactions among azobenzene *cis*-isomers also play a crucial role in determining the SPR property of the LC-NPs. The strength of solvophobic and dipolar coupling effects in the given solvent depends on the chemical environment of the azobenzene core present in the monolayer shell. Thus, the ability to modulate the optical property of the LC-NP composite via external stimuli (UV irradiation) provides an excellent opportunity for various technological endeavors. [22p-r]

Chapter IV: Preparation, Structural Elucidation and Functional Properties of Metal-Ligand Coordination Polymers and a reduced graphene oxide composite

This Chapter describes the preparation and characterization of novel COPs, as well as a reduced graphene oxide (rGO) composite of a COP, derived from o-diimine (tetraamine) ligand (N4 donor) and metal ions. The designed target COPs have been realized by using two different tetraamines viz., 3,3'-diaminobenzidine (DAB) and 1,2,4,5-benzenetetramine (BTA) and metal salts namely, copper(II) acetate ($Cu(OAc)_2$), palladium(II) chloride ($PdCl_2$), zinc acetate ($Zn(OAc)_2$), cadmium(II) acetate ($Cd(OAc)_2$), gadolinium(III) acetate ($Gd(OAc)_3$) and praseodymium(III) acetate ($Pr(OAc)_3$). In essence, three functionally different COPs have been realized and presented under sections IV.2, IV.3, and IV.4. The preparation and characterization of a new Cu(II) COP formed by treating the BTA ligand with $Cu(OAc)_2$ have been portrayed under section IV.2. The synthesis, structural revelation, and the composite formation ability of a Pd(II) COP derived from the combination BTA ligand and $PdCl_2$ have been rendered in section IV.3. In section IV.4, the preparation of four photoluminescent COPs, by treating Zn(II), Cd(II), Gd(III) and Pr(III) ions with BTA ligand, and characterization along with their ability to sense the high energy materials (HEMs) and metal ions have been presented.

IV.1. Coordination polymers: An overview

This part of the thesis introduces the readers to coordination polymers. It deals with the definition, molecular structure, classification, and various characteristic properties exhibited by these COPs. This also briefly covers the relationship between molecular structure, involving different ligands and metal ions, and multiple properties.

IV.2. Two-dimensional layered Cu(II) COP and multifunctional properties

This section describes a straightforward, gram-scale synthesis, electrical conductivity, redox behavior, thermoelectric properties, and magnetism of a two-dimensional (2D) layered copper(II) COP. The COPs, because of their diverse topological order coupled with coordination geometries, display a wide range of promising functional properties, including

adsorption/separation, catalysis, molecular recognition, magnetism, nonlinear optics, and electrical conductivity, host−guest behavior, thermoelectricity, luminescence, etc.[5] However, one of the most noticeable shortcomings of COPs is their low electrical conductivity (σ). As a result, their projected usage as sustainable media in batteries, fuel cells, capacitors, molecular wires, and so on remains unexplored. Similarly, their thermal conductivity, being the outcome of heat mobility by charge carriers, is also imperceptible, which is not surprising as this behavior is interlinked with electrical conductivity as well as the Seebeck coefficient.[5o] Nevertheless, another notable phenomenon observed in COPs is magnetism. Magnetically active frameworks generally comprise magnetic moment carriers such as paramagnetic metals (V, Cr, Mn, Fe, Co, Ni & Cu) and /or open-shell organic (radical) ligands. In the present day scenario, especially in microelectronics, spintronics, medical diagnosis, data storage devices, etc., there is an apparent demand for developing multifunctional COPs capable of exhibiting long-range charge transport as well as magnetic ordering.[5s,t] However, to our knowledge, the pristine (undoped) COPs exhibiting such combined properties have not been realized hitherto.

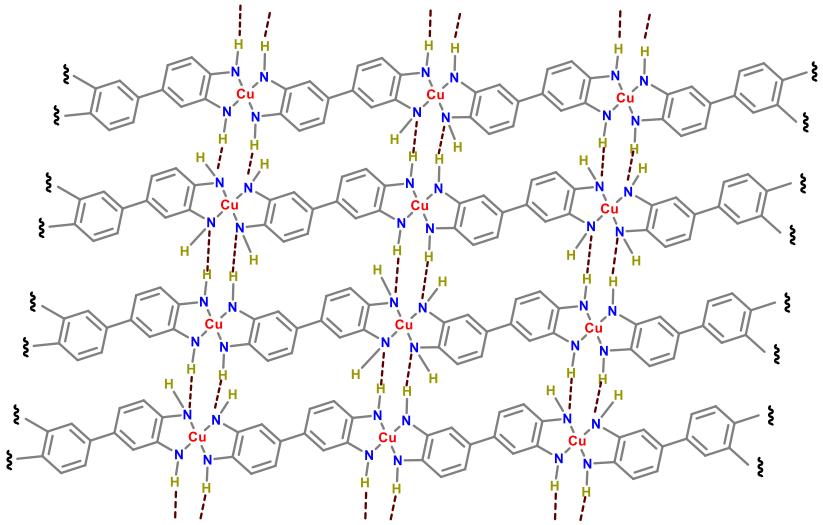

Most importantly, multi-characteristic COPs to be used in device applications need to be highly resistant to heat, moisture and air, inexpensive, and industrially scalable. Thus, there is an existent challenge to design and attain industrially scalable multifunctional COPs. The literature survey shows that the metal complexes derived from the family of o-diimine ligands (N4 donors) and transition metals (M = Cu, Ni, Zn, Pd, Pt, etc.) have the ability to address the concerns mentioned above. Moreover, it has been pointed out that the polymeric analogs of these complexes (COPs) may have added advantages as compared to their monomeric counterparts. Thus, we intended to design and develop new polymeric materials incorporating Cu(II) and o-diimine ligand as repeating units. The target COP was readily prepared on a large scale by simply treating DAB ligand with copper(II) acetate monohydrate, $Cu(OAc)_2 \cdot H_2O$ at room

temperature. The molecular structure of the newly prepared Cu(II) COP, hereafter referred to as **Cu(DAB)** for ease of presentation, has been shown below.

FTIR spectroscopy, Raman spectral analyses, microanalytical data, SEM-EDX imaging, surface analysis by XPS/AFM, powder X-ray diffraction, and HRTEM suggest a neutral 2D COP with Cu(DAB) repeating units. The experimental observations show that the COP stored under ambient conditions remains intact, exhibiting resistance to air, light, heat, water, and alkaline aqueous solution. While the AC experiments completely rule out ionic conductivity, two-probe DC electrical conductivity measurements on a pellet (bulk sample) as a function of temperature (150−320 K) evidence the electrical conductivity of the COP. Notably, at room temperature (298 K) the conductivity was found to be 0.01 S/m. Hall effect experiments revealed the intrinsic p-type conduction. Apart from being redox-active, it shows a thermoelectric property. Magnetic susceptibility vs. temperature measurements reveals the spin crossover from diamagnetic to the paramagnetic state upon cooling the bulk sample.

IV.3. Partially reduced composite for HER electrocatalysis derived from the Pd(II) COP

This section portrays the synthesis, characterization, and electrocatalytic activity for hydrogen evolution reaction (HER) of a novel reduced composite formed by subjecting to a partial reduction of a material resulting from the reaction of BTA ligand with $PdCl_2$ in the presence of reduced graphene oxide (rGO). For a comparative study, several closely related materials have been prepared and characterized. This research project was undertaken given the global environmental concerns related to the energy crisis. Currently, compared to other resources viz., natural gas, oil, and coal, the H_2 generation from water (splitting) electrolysis appears to be eternal and cost-effective. For the HER from water splitting, an efficient and stable electrocatalyst is absolutely obligatory. The eventual specific use of an electrocatalyst for the HER largely depends on its durability (robustness), ability to maximally lower the overpotential of an electrochemical reaction, and cost of synthesis (production).[24,25] COPs are gaining a great deal of attention in energy production and storage, particularly hydrogen storage and evolution, as they possess high specific surface area and metal centers favoring electrocatalytic HER.[26] Therefore, we intended to design and develop new materials derived from COPs capable of exhibiting HER electrocatalytic properties. Thus, a new COP-rGO composite has been conveniently prepared by treating BTA ligand with $PdCl_2$ in the presence rGO, and subjected to borohydride reduction to generate a novel electrocatalyst, which is denoted as **[Pd(BTA)-rGO]$_{red}$** for convenience. The analogous materials such as **Pd(BTA)**, **Pd(BTA)-rGO**, **Pd-rGO** and **[Pd(BTA)]$_{red}$** prepared for comparative investigations. The structural representations of these newly realized materials have been shown below in Scheme-I.

The **[Pd(BTA)-rGO]$_{red}$** composite thus prepared, unlike the similar materials realized and evaluated, exhibits an exceptional electrochemical activity for HER, affording a current density of -10 mA / cm^2 at the low overpotential of -127 mV with the Tafel slope value of 55 mV/dec and high durability (70 h at -300 mA/cm^2). The probing of this inexpensive composite with the aid of various techniques reveals the occurrence of Pd NPs of size ~ 3-5 nm encapsulated within the wide-surface-area of 2D sheets (layers), contributing significantly to the excellent HER performance of the catalyst. Encapsulation of Pd NPs over the 2D layers, formed by self-assembly of rigid COP frameworks, enhances the stability by preventing the aggregation and sintering of Pd NPs. In essence, the findings of this work, which primarily involves a facile route to the generation of catalytically active Pd NPs through the COP-rGO composite, appears to provide a promising approach for the design and fabrication of a wide range of inexpensive hybrid materials for various applications.

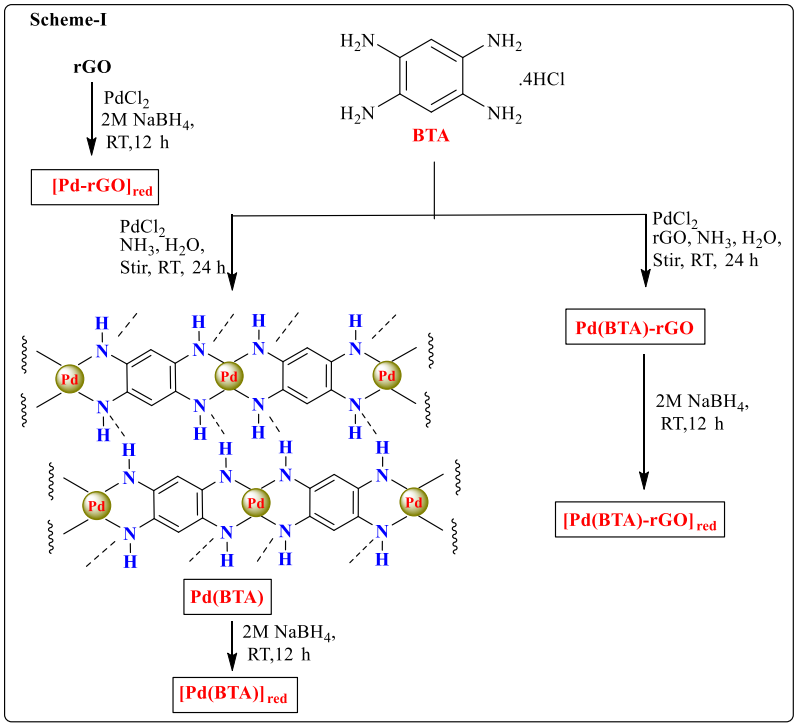

IV.4. Fluorescent COPs for explosive and metal ion detections

The preparation and characterization of four new fluorescent COPs and their intrinsic ability to act as "turn-off" luminescent sensors toward explosives and toxic mercury ions have been described in this section. Explosives, falling under the high energy materials (HEMs) category, are hazardous substances posing threats to national/international security and civil society.[27a,b] Moreover, they are proven to inflict multi-organ life-threatening injuries and pollute/damage the environment. Similarly, the toxic element contaminants in-ground or surface drinking water pose a considerable threat to living beings.[27c-e] Therefore, in recent years, the

process of on-field, ultra-fast sensing/detection of explosives and heavy metal ions has become the focal point of both researchers and technologists.[27f-q] There has been a tremendous increase in research within this arena where constant efforts have been made to develop new/innovative techniques or improve the existing methods or sensing devices (sensors). Amongst many forms reported hitherto, luminescence sensing[27l-q] appears to be the most economical and efficient technique for rapidly detecting such analytes. In this simple detection method, which can be regarded as the opposite of the colorimetric approach, measurable fluorescence quenching occurs. The intensity of light emitted by the sensitive fluorescent indicator (chemosensor) gets considerably reduced by the analyte. However, the fluorescent chemosensors have several concerns, such as their economic feasibility, ease of use, reusability, chemical/thermal stability, sensitivity, selectivity, detection limit, accuracy, etc.[27m,n]

In recent years, it is shown that the luminescent COPs and MOFs, as the fluorescent chemosensors, have unique structural compositions that are highly promising and competent in addressing the issues mentioned earlier.[4o] But, it appears that the COPs, when compared to MOFs, have been explored to some extent, and thus efforts have to be put-in to design and prepare new fluorescent COPs. Accordingly, four new photoluminescent COPs have been prepared by treating BTA ligand with $Zn(OAc)_2$, $Cd(OAc)_2$, $Gd(OAc)_3$) and $Pr(OAc)_3$ at room temperature. The newly prepared COPs viz., **Zn(BTA)**, **Cd(BTA)**, **Gd(BTA)** and **Pr(BTA)** have been fully characterized in terms of their molecular and sensing capabilities. The results of different spectroscopic data coupled with elemental analysis evidence the 2D structure of the COPs. A general structure representing all the four 2D COPs realized in this study is shown below.

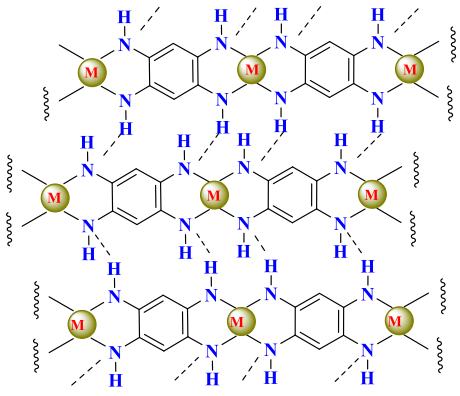

Zn(BTA): M = Zn(II); **Cd(BTA)**: M = Cd(II)
Gd(BTA): M = Gd(III); **Pr(BTA)**: M = Pr(III)

The luminescence properties of the four new COPs prepared have been measured using their millimolar (mM) solutions at room temperature. Fluorescence titration has been carried out for different explosives, including nitroaromatics (NACs) and nonaromatics (aliphatics). For

each titration, the mM solutions of both COPs and analytes (explosives and mercury salt) of known concentrations were prepared. Subsequently, the analyte solutions were added to the solutions of COP sensors progressively, and the corresponding emission spectra were recorded. The results revealed that the interaction of COP fluorophores with NACs is more appealing than that of the aliphatic analytes. Among all of the NACs used, 2,4,6-trinitrophenol (TNP) (picric acid) showed the complete fluorescence quenching efficiency of all the four COP fluorophores. Of these, the highest efficiency with the detection limit as low as 0.1 μM for TNP, was observed in the case of **Gd(BTA)** . Notably, apart from sensing explosives, these COPs detect Hg(II) ions in water samples with high selectivity and sensitivity reaching to parts per billion (ppb) level. In essence, the COPs synthesized in the present study can be used for practical applications given their production coast, stability, sensitivity and selectivity.

.

References:

(1) (a) Tiwari, A.; Uzun, L. (Eds), *Advanced Functional Materials*, Scrivener Publishing LLC, Wiley-VCH (2015)
(b) Md. Arifur , R.; Samantha, L. K.; Shuaijun, P.; Joseph, J. R.; Frank, C. *Angew.Chem. Int. Ed*., **2019**, 58,1904 –1927.
(c) Meng-Meng, S.; Ya-Min, W.; Xiang-Yong, L.; Xiao-Qin, Z.; Sheng, Z.; Bang-Jing, L. *Soft Matter*, **2019**, 15, 6615-6625.
(d) Jingpei, H.; Huawen, H.; Min, Z.; Xiaohong, H.; Min, C.; Dongchu, C.; Jinwen, L.; Guifeng, X.; Yang, W.; Zhongliu, W. *RSC Adv*., **2017**, 7, 2281-2287.

(2) (a) Rao, C. N. R.; Achim M.; Cheetham, A. K. (Eds), *The Chemistry of Nanomaterials: Synthesis, Properties and Applications*. John Wiley & Sons, **2006**.
(b) Manisha, S.; Anurag, S.; Sudip, M. *Nano Express*, **2020**, 1, 012003.
(c) Riddhiman, M.; Maria, D. M.; Randall, L. *ACS Appl. Nano Mater*. **2020**, 3, 6156–6185.

(3) (a) Rodriguez, J.A. Fernandez-Garcia, M. (Eds.) *Synthesis, Properties and Applications of Oxide Nanoparticles*. Whiley: New Jersey, **2007**.
(b) Corr, S. A. *Metal oxide nanoparticles; Nanoscience: Volume 1: Nanostructures through Chemistry*, RSC Publishing, **2012**, *1*, 180-207.
(c) Hurst,; Sarah, J. (Eds) (2011-01-01). Nanoparticle Therapeutics: FDA Approval, Clinical Trials, Regulatory Pathways, and Case Study - Springer. Methods in Molecular Biology, Humana Press, **2011**.
(d) Hewakuruppu, Y. L.; Dombrovsky, L. A.; Chen, C.; Timchenko, V.; Jiang, X.; Baek, S.; Taylor, R. A. *Applied Optics* **2013**, 52 (24): 6041–6050.
(e) Michelle, P.**;** Zdeněk, S.; Martin, P. *Energy Environ. Sci*., **2019**, 12, 41-58.
(f) Yang, S.; Shaohua, G.; Haoshen, Z. *Energy Environ. Sci*., **2019**,12, 825-840.
(g) Keke, H.; Yu, S.; Yuan, Z.; Xiyang, W.; Wei, Z.; Shouhua, F. *Adv. Mater*. **2019**, 31, 1801430.

(4) (a) Batten, S. R.; Neville, S. M.; Turner, D. R. *Coordination Polymers: Design, Analysis and Application*, RSC, Cambridge, **2009**.
(b) Janiak, C. *Dalton Trans*. **2003**, 2781-2804 and references cited there.
(c) Robin, A. Y.; Fromm, K. M. Coordination polymer networks with O- and N-donors: What they are, why and

how they are made. *Coordin. Chem. Rev*. **2006**, *250*, 2127–2157.
(d) For excellent review articles, see the special issue devoted to *Metal Organic Frameworks*, *Chem. Soc. Rev*. **2009**, 38.
(e) Yamada, T.; Otsubo, K.; Makiurac, R.; Kitagawa, H. *Chem. Soc. Rev*. **2013**, *42*, 6655-6669.
(f) Cheetham, A. K.; Rao, C. N. R.; Feller, R. K. *Chem. Commun*. **2006**, 4780–4795.
(g) Spokoyny, A. M.; Kim, D.; Sumrein, A.; Mirkin, C. A. *Chem. Soc. Rev*. **2009**, *38*, 1218–1227.
(h) Givaja, G.; Amo-Ochoa, P.; Gomez-Garcia, C. J.; Zamora, F. *Chem. Soc. Rev*. **2012**, *41*, 115-147.
(i) Rurack, K.; Martinez-Manez, R. (Eds), *The Supramolecular Chemistry of Organic-Inorganic Hybrid Materials*. Wiley, Hoboken, **2010**.
(j) Kitagawa, S.; Kitaura, R.; Noro, S. *Angew. Chem., Int. Ed*. **2004**, *43*, 2334-2375.
(k) Maeda, H.; Sakamoto, R.; Nishihara, H. *Langmuir* **2016**, *32*, 2527−2538.
(l) Qi, W.; Didier, A. *Chem. Rev*., **2020**, 120, 2, 1438–1511.
(m) Victoria, R. *Nature Reviews*, **2017**, 1, 0018.
(n) Hong, Z.; Ximeng, L.; Yue, W.; Cao, G.; Anthony, K. C.; John, W. *Chem. Commun*., **2018**, *54*, 5268-5288.
(o) Lustig, W. P.; Mukherjee, S.; Rudd, N. D.; Desai, A. V.; Li, J.; Ghosh, S. K. *Chem. Soc. Rev*., **2017**, *46*, 3242–3285.

(5) (a) Batten, S. R. *Pure Appl. Chem*. **2013**, *85*, 1715–1724.
(b) Davis, M. E. *Nature* **2002**, *417*, 813-821.
(c) Stock, N.; Biswas, S. *Chem. Rev*. **2012**, *112*, 933–969.
(d) Czaja, A. U., Trukhan, N.; Muller, U. *Chem. Soc. Rev*. **2009**, *38*, 1284–1293.
(e) McGuire, C. V.; Forgan, R. S. *Chem. Commun*. **2015**, *51*, 5199-5217.
(f) Kreno, L. E. *Chem. Rev*. **2012**, *112*, 1105–1125.
(g) Campbell, M. G.; Sheberla, D.; Liu, S. F.; Swager, T. M.; Dinca, M. *Angew. Chem. Int. Ed*. **2015**, *54*, 4349–4352.
(h) Alexandrov, E. V.; Virovets, A. V.; Blatov, V. A.; Peresypkina, E. V. *Chem. Rev*. **2015**, *115*, 12286−1231
(i) Sheberla, D. *J. Am. Chem. Soc*. **2014**, *136*, 8859−8862.
(j) Stavila, V.; Talin, A. A.; Allendorf, M. D. *Chem. Soc. Rev*. **2014**, *43*, 5994-6010.
(k) Darago, L. E.; Aubrey, M. L.; Yu, C. J.; Gonzalez, M. I.; Long, J. R. *J. Am. Chem. Soc*. **2015**, *137*, 15703−15711.
(l) Kiley, A. W.; Demetra, A. C.; Kristy, A. G.; Jack, S.; Nathaniel, L. R.; Stéphane, P. *J. Am. Chem. Soc*. **2009**, 131, 50, 18069–18071.
(m) Qiangsheng, Z.; Jun, W.; Alexander, M. K.; Wei, D.;, Cong, X.; Cailing, X.; Lizi, Y.; Ran, F.; Weisheng, L. *ACS Appl. Mater. Interfaces*, **2018**, 10, 28, 23976–23986.
(n) Yang, L.; Xiao-Yu, X.; Chen, C.; Zhen-Shu, S.; Huai-Song, W. *J. Mater. Chem. C*, **2019**, 7, 10743-10763.
(o) Engelbert, R.; Helmut, B. *APL Materials*, **2020**, 8, 060902.
(p) Maria de, L. G.; Eduardo, F.; Marisol, M.; Iris, N.; Darren, B. *J. Mater. Chem. A*, **2020**, 8, 13197-13206.
(q) Byeonggwan, K.; Jongbeom, N.; Hanwhuy, L.; Younghoon, K.; Jinbo, K.; Eunkyoung, K. *Adv. Funct. Mater*. **2018**, 1807549.
(r) Eugenio, C.; Guillermo, M. E. *Chem. Soc. Rev*., **2013**, 42, 1525-1539.
(s) Guillermo, M. E.; Eugenio, C. *Chem. Soc. Rev*., **2018**, 47, 533-557.
(t) Xun, F.; Yapei, S.; Heng, Z.; Rongfang, L.; Weizhou, W.; Daoming, Z.; Liya, W.; Zhongjun, L. *RSC Adv*., **2019**,9, 16328-16338.

(6) (a) Dinga, S.-Y.; Wang,W. *Chem. Soc. Rev*. **2013**, *42*, 548-568.
(b) Huang, N.; Wang, P.; Jiang, D. *Nature Rev. Mater.* **2016**, *1*, 16068.
(c) Maria, S. L.; Thomas, B. *Adv. Funct. Mater*. **2018**, 28, 1705553.

(d) Xinyu, G.; Hui, L.; Yunchao, M.; Ming, X.; Qianrong, F.; Yushan, Y.; Valentin, V.; Shilun, Q. *Nature Chemistry*, **2019**, 11, 587–594.
(e) Shushan, Y.; Xin, L.; Junyong , Z.; Gang, Z.; Peter, V. P.; Bart Van der B. *Chem. Soc. Rev*., **2019**, 48, 2665-2681.
(f) Sharath, K.; Kaushik, D.; Rahul, B. *J. Am. Chem. Soc*. **2019**, 141, 5, 1807–1822.
(g) Priv, D.; Florian, B.; Bappaditya, G. *Angew.Chem. Int.Ed*. **2018**, 57,4850 –4878.

(7) (a) Goodby, J. W.; Collings, P. J.; Kato T.; Tschierske C.; Gleeson, H.; Raynes, P. (Editors), *Handbook of Liquid Crystals*. ***Volume 1****: Fundamentals of Liquid Crystals*, 2nd Edition, Wiley-VCH, Germany, **2014**.
(b) Goodby, J. W.; Collings, P. J.; Kato T.; Tschierske C.; Gleeson, H.; Raynes, P. (Editors), *Handbook of Liquid Crystals*. ***Volume 2****: Physical Properties and Phase Behavior of Liquid Crystals*, 2nd Edition, Wiley-VCH, Germany, **2014**.
(c) Goodby, J. W.; Collings, P. J.; Kato T.; Tschierske C.; Gleeson, H.; Raynes, P. (Editors), *Handbook of Liquid Crystals*. ***Volume 3:*** *Nematic and Chiral Nematic Liquid Crystals*, 2nd Edition, Wiley-VCH, Germany, **2014**.
(d) Goodby, J. W.; Collings, P. J.; Kato T.; Tschierske C.; Gleeson, H.; Raynes, P. (Editors), *Handbook of Liquid Crystals*. ***Volume 4****: Smectic and Columnar Liquid Crystals*, 2nd Edition, Wiley-VCH, Germany, **2014**.
(e) Goodby, J. W.; Collings, P. J.; Kato T.; Tschierske C.; Gleeson, H.; Raynes, P. (Editors), *Handbook of Liquid Crystals*. ***Volume 5****: Nonconventional Liquid Crystals*, 2nd Edition, Wiley-VCH, Germany, **2014**.
(f) Goodby, J. W.; Collings, P. J.; Kato T.; Tschierske C.; Gleeson, H.; Raynes, P. (Editors), *Handbook of Liquid Crystals*. ***Volume 6****: Nanostructured and Amphiphilic Liquid Crystals*, 2nd Edition, Wiley-VCH, Germany, **2014**.
(g) Goodby, J. W.; Collings, P. J.; Kato T.; Tschierske C.; Gleeson, H.; Raynes, P. (Editors), *Handbook of Liquid Crystals*. ***Volume 7****: Supermolecular and Polymeric Liquid Crystals*, 2nd Edition, Wiley-VCH, Germany, **2014**.
(h) Goodby, J. W.; Collings, P. J.; Kato T.; Tschierske C.; Gleeson, H.; Raynes, P. (Editors), *Handbook of Liquid Crystals*. ***Volume 8****:* Applications of Liquid Crystals, 2nd Edition, Wiley-VCH, Germany, **2014**.

(8) (a) Serrano, J. L. (Ed.), Metallomesogens *: Synthesis, Properties and Applications*, Wiley-VCH, Germany, **2010**.
(b) Josefina, J.; José A. Z.; José L. S.; Joaquín, B.; Luis, O. *Inorg. Chem*. **2020**, 59, 7, 4842–4857.
(c) Raquel, G.; Olga, C.; Beatriz, D.; Anabel, E. *J. Mater. Chem. C,* **2020**, 8, 6552-6557.
(d) Ryohei, A.; Yuma, H.; Daisuke, K.; Mayu, T.; Masaaki, N.; Leonard, F. L.; Shinya, H. *Chem. Sci*., **2019**, 10, 5843-5848.
(e) Cristián, C.; José, A. C.; Mercedes, C.; Rainer, S. *J. Mater. Chem. C*, **2019**, 7, 10318-10330.
(f) Xiugang, W.; Mengbing, Z.; Bruce, D. W.; Weiguo, Z.; Yafei, W. *J. Mater. Chem. C*, **2018**, 6, 9848-9860.
(g) Cristián, C.; José, A. C.; Mercedes, C.; Carlos, L. *Chem. Eur.J*. **2019**, 25,12046 –12051.

(9) (a) Nealon, G. L.; Greget, R.; Dominguez, C.; Nagy, Z. T.; Guillon, D.; Gallani, J.-L.; Donnio, B. *Beilstein J. Org. Chem*. **2012**, 8, 349–370.
(b) Lagerwall, J. P. F.; Scalia, G. *Curr. Appl. Phys*. 2012, *12*, 1387e1412
(c) Li, Q. (Ed). *Nanoscience with Liquid Crystals: From Self-Organized Nanostructures to Applications (NanoScience and Technology)*, Springer, Switzerland, **2014**.
(d) Bisoyi, H. K.; Kumar, S. *Chem. Soc. Rev*. **2011**, *40*, 306.
(e) Yuriy, G.; Anatoly, G. *Nanomaterials*, **2017**, 7(11), 361.
(f) Sanat, K. K.; Venkat, G.; Robert, A. R. *J. Chem. Phys*. **2017**, 147, 020901.

(g) Ewelina, T.; Aleksander, P.; Maciej, B.; Ewa, G.; Michał, W. *Small*, **2019**, 15, 1902807.
(h) Ziyue, D.; Zihan, Y.; Zhenkun, Z.; Ke, X.; Pengjiao, Z. *Biomacromolecules*, **2020**, 21, 6, 2376–2390.
(i) Patricio, R. H.; Luz, J. M. M.; Ariel, M. F.; Eduardo, A. S. B. *Liq. Cryst*., **2020**, 47, 423-432.

(10) (a) Brenner, T. M.; Egger, D. A.; Kronik, L.; Hodes, G.; Cahen, D. *Nature Rev. Mater*. **2016**, *1*, 15007
(b) Lin, C.-F.; Su, W.-F.; Wu, C.-I.; Cheng, I.-C. Organic, *Inorganic and Hybrid Solar Cells: Principles and Practice*, Wiley-IEEE Press, **2012**.
(c) Xiuli, Y.; Jiaojiao, Y.; Zhenhong, W. *Dalton Trans*., **2020**, 49, 7252-7257.
(d) Yuheng, L.; Kesong, Y. *Energy Environ. Sci*., **2019**, 12, 2233-2243.
(e) Wenhui, F.; Zhibin, F.; Bo, W.; Lulu, Z.; Yan, Z.; Yu, Y.; Mianli, H.; Sunxian, W.; Ping, L. *J. Mater. Chem*. *A*, **2017**, 5, 1387-1393.
(f) Liang, M.; Jun, D.; Xiao, C. Z. *Adv. Energy Mater*. **2017**, 1601731.

(11) (a) Inzelt, G. (Ed), *Conducting Polymers: A New Era in Electrochemistry*, Springer, **2012**.
(b) Vidor, F. F.; Meyers, T. and Hilleringmann, U., *Electronics*, **2015**, *4*, 480-506
(c) Baolin, G.; Peter, X. M. *Biomacromolecules*, **2018**, 19, 6, 1764–1782.
(d) Aimee, M. B.; Luciano, M. S.; Yang, L.; Shinjita A.; Julio M. D. *Chem. Mater*. **2016**, 28, 17, 5989–5998.
(e) Christina, O. B.; Xinwei, H.; Wyatt, N.; Richard, B. K. *Chem. Soc. Rev*., **2017**, 46, 1510-1525.
(f) Jorge, G. I.; Marina, E. R.; Silvia, G. G.; M'hamed, C.; Oscar, A. J. Q.; Bernardo, A. F. U. *Chem. Rev*. **2018**, 118, 9, 4731–4816.
(g) Jhih-Guang, W.; Jie-Hao, C.; Kuan-Ting, L.; Shyh-Chyang, L. *ACS Appl. Mater. Interfaces*, **2019**, 11, 24, 21294–21307.
(h) Hyunwoo, Yuk.; Baoyang, Lu.; Shen, L.; Kai, Qu.; Jingkun, X.; Jianhong, L.; Xuanhe, Z. *Nature Communications*, **2020**, 11, 1604.
(i) Akihisa, I.; Hyunwoo, Y.; Baoyang, Xuanhe, Z. *Science Advances*, **2020**, 12, 5394.

(12) (a) Jorio, A.; Dresselhaus, G.; Dresselhaus, M. S. *Carbon Nanotubes: Advanced Topics in the Synthesis, Structure, Properties and Applications*, **2008**.
(b) Meyyappan, M. *Carbon Nanotubes: Science and Applications*, CRC Press, **2004**
(c) Steffen, F. H.; Anna, L. *Nature Nanotechnology*, 2020, 15, 3-4.

(13) (a) Warner, J. H.; Schäffel, F.; Rummeli, M. H.; Bachmatiuk, A. Graphene: Fundamentals and emergent applications, Elsevier Inc. **2013**.
(b) Rao, C. N. R.; Sood, A. K. Graphene: Synthesis, Properties, and Phenomena, Wiley-VCH Verlag, **2013**

(14) (a) Chandrashekar, S.; Sadashiva, B.K. Suresh, K. A. *Pramana*. **1977**, *9*, 471.
(b) Pruthvi, M.; Asmita, S.; Swamynathan, K.; Dharmendra, P. S.; Redouane, D.; Sandeep, K. *J. Mater. Chem. C*, **2020**,8, 9252-9261.
(c) Baomin, Z.; Bo, L.; Rui, Q. P.; Kai, Z.; Kheng, A. L.; Jing, L.; Jinjun, S.; Peter, K. H. H.; Chunyan, C.; Jishan, W. *Chem. Mater*. **2010**, 22, 2, 435–449.
(d) Yelamaggad, C.V.; Achalkumar, A. S.; Shankar Rao, D. S.; Krishna Prasad, S. *J. Org. Chem*., **2007**, 72, 22, 8308–8318.
(e) Christine, L.; Johan F. E.; Vance E. W. *J. Am. Chem. Soc*., **2008**, 130, 35, 11791–11800.
(f) Yelamaggad, C.V.; Achalkumar, A. S.; Shankar Rao, D. S.; Mitsunori, N.; Hiroki, A.; Jun-ichi, Y.; Shin'ichi, N. *J. Mater. Chem*., **2008**,18, 3433-3437.
(g) Asmita, S.; Benoit, D.; Ashwathanarayana , G.; Sandeep, K.; Matthieu, B.; Carine, D.; Christian, L.; Redouane, D.; Dharmendra , P. S. *New J. Chem*., 2020, Accepted Manuscript.

(h) Hongbing, P.; Wei, Z.; Anqi, X.; Xiaolin, L.; Pingping, H.; Zhihao, S.; Xinghe, F. *Polym. Chem*., **2019**,10, 991-999.

(15) (a) Kitzerow, H. S.; Bahr, C. *Chirality in Liquid Crystals*, Springer-Verlag, New Yark, **2001.**
(b) Goodby, J. W.; Waugh, M. A.; Stein, S. M.; Chin, E., Pindak, R.; Patel, J. S., Nature, **1989**, *337*, 449.
(c) Goodby, J. W.; Waugh, M. A.; Stein, S. M.; Chin, E.; Pindak, R; Patel, J. S. J Am. Chem. Soc., 1989b, *111*, 8119.
(d) Vidhika, P.; Golam, M.; Supreet, K.; Raj Kumar, K.; Sharmistha, G.; Santanu Kumar, P. *Chem. Commun*. **2018**,54, 3452-3455.
(e) Susanta, C.; Malay Kumar, D.; Alexej, B.; Wolfgang, W.; Dorota, W.; Roman, D. *J. Mater. Chem. C*, **2019**,7, 10530-10543.

(16) (a) Demus, D. *Liq. Crys*. **1989**, *5*, 75
(b) Tschierske, C. *J. Matter. Chem*. **1998**, *8*, 1485
(c) Tschierske, C. *J. Matter. Chem*. **2001**, *11*, 2647
(d) Tschierske, C. *Annu. Rep. Prog. Chem., Sect*. C. **2001**, *97*, 191
(e) Tschierske, C. *Curr. Opin. Colloid Interface Sci*. **2002**, *7*, 69

(17) (a) Nguyen, H. T.; Destrade, C.; Malthete, J. *Adv. Mater*. **1997**, *9*, 375.
(b) Malthete, J.; Nguyen, H. T.; Destrade, C. *Liq. Cryst*. **1993**, *13*, 171.
(c) Xiongwei, P.; Hongfei, G.; Yulong, X.; Huifang, C.; Fanran, H.; Xiaohong, C. *New J. Chem*., **2017**,41, 2004-2012.
(d) Jianchuan, T.; Rong, H.; Hongfei, G.; Xiaohong, C.; Marko, P.; Tschierske, C. *RSC Adv*., **2012**, 2, 2842-2847.
(e) Mohamed, A.; Silvio, P.; Tschierske, C. *Journal of Molecular Liquids*, **2019**, 227, 233-240.
(f) Leon, D.; Rodrigues, D.; Sunil, D.; Chaithra, P. B. *Journal of Molecular Liquids*, **2020**, 297, 111909.
(g) Subrata, N.; Suraj, K. P.; Joydip, D.; Santanun Kumar, P.; Achalkumar, A. S. *Mol. Syst. Des. Eng*., **2017**,2, 478-489.

(18) (a) Niori, T.; Sekine, T.; Watanabe, J.; Furukawa, T.; Takezoe, H. *J. Mater. Chem*. **1996**, *6*, 1231.
(b) Pelzl, G.; Diele, S.; Weissflog, W. *Adv. Mater*. **1999**, *11*, 707.
(c) Fodor-Csorba, K.; Vajda, A.; Galli, G.; Jakli, A.; Demus, D.; Holly, S.; Gacs-Batiz, E. *Macro. Chem. Phys*. **2002**, *203*, 1556.
(d) Rafael, V.; Paul, L.; Seung, H. H.; John, H.; Elaine, D.; Peter, P. M.; Michael, K.; Samuel, S.; Jim, T. G.; Antal, J. *J. Mater. Chem*. **2010**,20, 8488-8495.
(e) Khana, R. K.; Turlapati, S.; Begum, N.; Mohiuddin, G.; Rao, N. V. S.; Ghosh, S. *RSC Adv*. **2018**, 8, 11509-11516.
(f) Ashwathanarayana, G.; Litwin, J.; Nithin, J.; Reji, P.; Pratibha, R.; Sandeep, K. *New J. Chem*. **2018**, 42, 2047-2057.
(g) Sithara, P. S.; Yuri, P. P.; Jagdish, J. K.; Vitaly, P. P.; Anne, L.; Marco, P.; Marko, P.; Carsten, T. *Nature Communications*, **2016**, 7, 11369.

(19) (a) Imrie, C. T. *Structure and Bonding - Liquid crystals, II*, Springer-Verlag., **1999**.
(b) Imrie, C. T.; Henderson, P. A. *Curr. Opin. Colloid Interface Sci*. **2002**, *7*, 298.
(c) Imrie, C. T.; Henderson, P. A. *Chem. Soc. Rev*, **2007**, *36*, 2096.
(d) Imrie, C. T.; Luckhurst, G. R. *Handbook of liquid crystals. Vol-2B*, Weiley-VCH, Germany. **1998**

(e) Yelamaggad, C. V.; Shanker, G.; Hiremath, Uma S.; Krishna Prasad, S. *J. Mater. Chem.* **2008**, *18*, 2927 and references cited therein
(f) Pal, S. K.; Kumar, S. Liquid Crystal Dimers, Cambridge University Press, UK, **2017** and referenced therein
(g) Hardouin, F.; Achard, M. F.; Jin, J. -I.; Shin, J.-W.; Yun, Y.-K. *J. Phys. II*. **1994**, *4*, 627.
(h) Yelamaggad, C. V. *Mol. Cryst. Liq. Cryst*. **1999**, *326*, 149.
(i) Yelamaggad, C.V. ; Krishna Prasad, S. ; Nair, G. G. ; Shashikala, I.; Shankar Rao, D. S. ; Lobo, C. V. ; Chandrasekhar, S. *Angew. Chem. Int. Ed*. **2004**, *43*, 3429.
(j) Padmini Tamilenthi, V.; Nani Babu, Nair, G. G.; Shankar Rao, D. S.; Yelamaggad, C. V., *Chem. Asian J*., **2106**, *11*, 2897–2910
(k) Yelamaggad, C. V.; Shashikala, I.; Hiremath, U. S.; Shankar Rao, D. S. ; Krishna Prasad, S. *Liq. Cryst*. **2007**, *34*, 153.
(l) Cha, S. W. Jin, J.-I.; Achard, M. F.; Hardouin, F., *Liq. Cryst*. **2002**, *29*, 755.
(m) Yuki, A.; Hideto, T. *Journal of Molecular Liquids*, **2019**, 289, 111097.
(n) Daniel, A. P.; Jordan, P. A.; William, H.; John, S.; Corrie, T. I. *Liq. Cryst*, **2017**, 44,127.
(o) Klaudyna, K.; Tomasz, J.; Agnieszka, M. N.; Damian, P.; Ewa, G.; Ziauddin, A.; Chris, W.; Georg, H. M.; Adam, P.; Robert, N. *Nanoscale*, **2018**,10, 16201.
(p) Rashmi, A. N.; Sachin, A. B.; Shanker, G.; Shankar Rao, D. S.; Yelamaggad, C. V. *New J. Chem*., **2019**,43, 2148

(20) (a) Quan, Li (Ed). *Nanoscience with Liquid Crystals: From Self-Organized Nanostructures to Applications (NanoScience and Technology)*, Springer, Switzerland, **2014**.
(b) Dobbs, W.; Suisse, J.-M.; Douce, L.; Welter, R. *Angew. Chem. Int. Ed*. **2006**, *45*, 417
(c) Draper, M.; Saez , I. M.; Cowling, S. J.; Gai , P.; Heinrich, B.; Donnio, B.; Guillon, D.; Goodby, J. W. *Adv. Funct. Mater*. **2011**, *21*, 1260–1278.
(d) Sajanlal, P. R.; Sreeprasad, T. S.; Samal, A. K.; Pradeep, T. *Nano Reviews*. **2011**, *2*, 5883. (e) Bisoyi, H. K.; Kumar, S. *Chem. Soc. Rev*. **2011**, *40*, 306. (f) Lagerwall, J. P.F.; Scalia, G. *Curr. Appl. Phy*. **2012**, *12*, 1387.
(g) Dintinger, J.; Tang, B.-J.; Zeng, X.; Liu, F.; Kienzler, T.; Mehl, G. H.; Ungar, G.; Rockstuhl, C.; Scharf, T. *Adv. Mater*. **2013**, *25*, 1999–2004.
(h) Nealon, G. L.; Greget, R.; Dominguez, C.; Nagy, Z. T.; Guillon, D.; Gallani, J.-L.; Donnio, B. *Beilstein J. Org. Chem*. **2012**, *8*, 349.
(i) Ou, J. Y.; Plum, E.; Jiang, L.; Zheludev, N. I. *Nano Lett*. **2011**, *11*, 2142-2144.
(j) Piotr, L.; Karolina, B.; Wiktor, L.; Michał, W.; Sylwia, P.; Maciej, B.; Tomasz, O.; Konrad, M.; Kamil, O.; Michał, M.; Jan, B.; Tomasz, R. W. *ACS Nano*, **2019**, 13, 9, 10154.
(k) Martin, U.; Javad, M.; Anshul, S.; Daniel, H.; Heinz-S, K.; Torsten, H. *Liq. Cryst*. **2016**, 43, 183.
(l) Changyeon, B.; Jong, H. U.; Ji Eun, W.; Chang, K. K.; Keon, J. L.; Kwi-Il, P.; Do Kyung, K. *Nanoscale*, **2016**,8, 17632-17638.
(m) Shcherbinin, D.P.; Konshina, E.A. *Liq. Cryst.* **2017**, 44, 648-655.
(n) Patricio, R. H.; Luz. J. M.; Ariel, M. F.; Eduardo, A. S. B. *Liq. Cryst.* **2020**, 47, 423-432.
(o) Amit, C.; Gautam, S.; Ashok, M. B. *Nanoscale*, **2014**,6, 7743-7756.
(p) Sandeep, K. *NPG Asia Materials*, **2014**, 6, e82.
(q) Yuan, Z.; Qingkun, L.; Haridas, M.; Yuan, Y.; Ivan, I. S. *ACS Nano*, **2015**, 9, 3, 3097–3108.

(21) (a) Grzelczak, M.; Pe´rez-Juste, J.; Mulvaney, P.; Liz-Marza´n, L. M. *Chem. Soc. Rev*. **2008**, *37*, 1783-1791.
(b) Wojcik, M.; Lewandowski, W.; Matraszek, J.; Mieczkowski, J.; Borysiuk, J.; Pociecha, D.; Gorecka, E. *Angew. Chem., Int. Ed*. **2009**, *48*, 5167-5169.

(c) Wojcik, M.; Kolpaczynska, M.; Pociecha, D.; Mieczkowski, J.; Gorecka, E. *Soft Matter* **2010**, *6*, 5397-5400.
(d) Zeng, X.; Liu, F.; Fowler, A. G.; Ungar, G.; Cseh, L.; Mehl, G. H.; Macdonald, J. E. *Adv. Mater*. **2009**, *21*, 1746-1750.
(e) Cseh, L.; Mehl, G. H. *J. Am. Chem. Soc*. **2006**, *128*, 13376-13377.
(f) Mischler, S.; Guerra, S.; Deschenaux, R. *Chem. Commun*. **2012**, *48*, 2183-2185.
(g) Yu, C. H.; Schubert, C. P. J.; Welch, C.; Tang, B. J.; Tamba, M.-G.; Mehl, G. H. *J. Am. Chem. Soc*. **2012**, *134*, 5076-5079.
(h) Mang, X.; Zeng, X.; Tang, B.; Liu, F.; Ungar, G.; Zhang, R.; Cseh, L.; Mehl, G. H. *J. Mater. Chem*. **2012**, *22*, 11101-11106.
(i) Donnio, B.; García-Va´zquez, P.; Gallani, J.-L.; Guillon, D.; Terazzi, E. *Adv. Mater*. **2007**, *19*, 3534-3539.
(j) Nealon, G. L.; Greget, R.; Dominguez, C.; Nagy, Z. T.; Guillon, D.; Gallani, J.-L.; Donnio, B. *Beilstein J. Org. Chem*. **2012**, *8*, 349-370.
(k) Marx, V. M.; Girgis, H.; Heiney, P.; Hegmann, T. *J. Mater.Chem*. **2008**, *18*, 2983.
(l) Vanessa, M. M.; Hidy, G.; Paul, A. H.; Torsten, H. *J. Mater. Chem*. **2008**,18, 2983-2994.
(m) Satya, P. Y.; Kanchan, Y.; Jayeeta, L.; Avanish, S. P. *Liq. Cryst. Rev.* 2018, 6, 143-169.
(n) Pushpavathi, N.; Sandhya, K. L. .; Pratibha, R. *Liq. Cryst.* 2019, 46, 666-673.
(o) Wan-Li, H.; Wei-Kai, Z.; Huan, Xu.; Li-Hao, L.; Zhou, Y.; Hui, C.; Dong, W.; Zhi-Gang, Z.; Huai, Y. *Phys. Chem. Chem. Phys*. **2016**, 18, 29028-29032.
(p) Liliana, C.; Xiaobin, M.; Xiangbing, Z.; Feng, L.; Georg, H. M.; Goran, U.; Giuliano, S. *J. Am. Chem. Soc*., **2015**, 137, 40, 12736–12739.

(22) (a) Gross, G. M.; Nelson, D. A.; Grate, J. W.; Synovec, R. E. *Anal. Chem*. **2003**, *75*, 4558.
(b) Dos Santos, D. S.; Goulet, P. J. G.; Pieczonka, N. P. W.; Oliveira, O. N.; Aroca, R. F. *Langmuir* **2004**, *20*, 10273
(c) Faulds, K.; Littleford, R. E.; Graham, D.; Dent, G.; Smith, W. E. *Anal. Chem*. **2004**, *76*, 592.
(d) Frederix, F.; Friedt, J.-M.; Choi, K.-H.; Laureyn, W.; Campitelli, A.; Mondelaers, D.; Maes, G.; Borghs, G., *Anal. Chem*. **2003**, *75*, 6894.
(e) Matsui, J.; Akamatsu, K.; Nishiguchi, S.; Miyoshi, D.; Nawafune, H.; Tamaki, K.; Sugimoto, N. *Anal. Chem*. **2004**, *76*, 1310.
(f) Tokareva, I.; Minko, S.; Fendler, J. H.; Hutter, E. *J. Am. Chem. Soc*. **2004**, *126*, 15950.
(g) Zhang, Z.-F.; Cui, H.; Lai, C.-Z.; Liu, L.-J. *Anal. Chem*. **2005**, *77*, 3324.
(h) Niidome, T.; Nakashima, K.; Takahashi, H.; Niidome, Y., *Chem. Commun*., **2004**, 1978.
(i) Hirsch, L. R.; Stafford, R. J.; Bankson, J. A.; Sershen, S. R.; Rivera, B.; Price, R. E.; Hazle, J. D.; Halas, N. J.; West, J. L. *Proc. Natl. Acad. Sci. U.S.A*. **2003**, *100*, 13549.
(j) Aslan, K.; Lakowicz, J. R.; Geddes, C. D. *Anal. Chem*. **2005**, *77*, 2007.
(k) Newman, J. D. S.; Blanchard, G. J. *Langmuir*, **2006**, 22, 13, 5882–5887.
(l) Faraday, M. *Philos. Trans. R. Soc. Lond*. **1857**, 147, 145–181.
(m) Abhijit, M.; Peng-Lei, C.; Haruhisa, A.; Tian-Xin, W.; Kaoru, T.; Wolfgang, K. *Chem. Mater*., **2003**, 15, 1, 20–28.
(n) Evgenii, T.; Liudmila, L.; Nino, L.; Andrei, V. K.; Peter, S.; Svetlana, S. *J. Phys. Chem. C*, **2015**, 119, 30, 17369–17377.
(o) Zonglin, C.; Yanxiao, H.; Tong, B.; Soumen, D.; Petr, K.; Rafal, K. *J. Am. Chem. Soc*., **2019**, 141, 5, 1949–1960.
(p) Sujit, K. G.; Tarasankar, P. *Chem. Rev*., **2007**, 107, 11, 4797–4862.
(q) Paresh, C. R. *Chem. Rev*., **2010**, 110, 9, 5332–5365.
(r) Wei, R.; Gungun, L.; Christian, C.; Jiajia, Z.; Dayong, J. *Adv. Mater*. **2020**, 32, 1901430.

(23) (a) Yelamaggad, C. V.; Shanker, G. *Liq. Cryst.* **2007**, *34*, 799.
(b) Achalkumar, A. S.; Shanar Rao, D. S.; Yelamaggad, C. V. *New J. Chem.* **2014**, *38*, 4235.
(c) Yelamaggad, C. V.; Shanker, G.; Hiremath, Uma S.; Krishna Prasad, S. *J. Mater. Chem.* **2008**, *18*, 2927.
(d) Pal, S. K.; Kumar, S. Liquid Crystal Dimers, Cambridge University Press, UK, **2017**.

(24) (a) Zhu, B.; Zou, R.; Xu, Q. *Adv. Energy Mater.* **2018,** *8* (24), 1801193.
(b) Shao, J.; Zhou, H.; Feng, J.; Zhu, M.; Yuan, A. *J. Alloys Compd*. **2019**, 784, 869−876.
(c) Feng, J.; Zhou, H.; Wang, J.; Bian, T.; Shao, J.; Yuan, A. *Int. J. Hydrogen Energy* **2018**, 43 (45), 20538−20545.
(d) Shao, J.; Feng, J.; Zhou, H.; Yuan, A. *Appl. Surf. Sci*. **2019**, 471, 745−752.

(25) (a) Yilmaz, G.; Yam, K. M.; Zhang, C.; Fan, H. J.; Ho, G. W. *Adv. Mater*. **2017**, 29 (26), 1606814.

(26) (a) Huang, Y.; Gao, S.; Liu, T.; Lü, J.; Lin, X.; Li, H.; Cao, R. *ChemPlusChem.* **2012,** *77* (2), 106-112.
(b) Lin, A.; Ibrahim, A. A.; Arab, P.; El-Kaderi, H. M.; El-Shall, M. *ACS Appl. Mater. Interfaces* **2017**, 9 (21), 17961−17968.
(c) Bernsmeier, D.; Chuenchom, L.; Paul, B.; Rümmler, S.; Smarsly, B.; Kraehnert, R. *ACS Catal*. **2016**, 6 (12), 8255−8263.

(27) (a) Marshall, M.; Oxley, J. C. (Eds.) Aspects of Explosives Detection, 2009, Oxford UK,
(b) Germain, M. E.; M. J. Knapp, *Chem. Soc. Rev*., **2009**, *38*, 2543–2555.
(c) James, W. R.; Greg, B. *Environ. Sci. Technol*. **2012**, 46, 729–736.
(d) Samraj, M.; Sahel, F.; Satyam, S.; Debanjan, M.; Sujit, K. G. *ACS Cent. Sci*. **2020**, 6, 1534–1541
(e) Hose, G. C.; Symington, K.; Lott, M. J.; Lategan, M. J. *Environmental Science and Pollution Research volume*, **2016**, 23, 18704-18713.
(f) S. A. Trammell, M. Zeinali, B. J. Melde, P. T. Charles, F. L. Velez, M. A. Dinderman, A. Kusterbeck and M. A. Markowitz, Anal. Chem. 2008, 80, 4627−4633; (g) X. B. Zhou, C. X. Yuan, D. D. Qin, Z. H. Xue, Y. L. Wang, J. Du, L. L. Ma, L. Ma and X. Q. Lu, Electrochim. Acta., 2014, 119, 243−250.
(h) R. D. Luggar, M. J. Farquharson, J. A. Horrocks and R. J. Lacey, X-Ray Spectrom., 1998, 27, 87–94.
(i) K. Hakansson, R. V. Coorey, R. A. Zubarev, V. L. Talrose and P. Hakansson, J. Mass Spectrom., 2000, 35, 337–346.
(j) J. M. Sylvia, J. A. Janni, J. D. Klein and K. M. Spencer, *Anal. Chem*., 2000, 72, 5834–5840.
(k) Sultan, B. J.; William, J. P. Raul, Q. C.; Christian, W. O. S.; Ioannis, P.; Ivan, P. P. *Nanoscale*, **2017**, 9, 16459-16466.
(l) Roberta, R.; Adolfo, G,.; Sergio, S.; Stefano, M. *Anal. Chem*. **2018**, 90, 4288–4292.
(m) Zhichao, H.; Benjamin, J. D.; Jing, L. *Chem. Soc. Rev*. **2014**,43, 5815-5840.
(n) Debasis, B.; Zhichao, H.; Jing, L. *Dalton Trans*., **2014**, 43, 10668-10685.
(o) Hui, X.; Fu, L.; Yuanjing, C.; Banglin, C.; Guodong, Q. *Chem. Commun*., **2011**,47, 3153-3155.
(p) Jason, C. S.; Antonio, G. D.; Arnold, L. R.; William, C. T. *Chem. Mater*. **2007**, 19, 6459–6470.
(q) André, R.; Alex, P. C.; Eugen, S.; Peter, T.; Andreas, P.; Patrick, G.; Ullrich, S.; Thomas, R. *Scientific Reports*, **2016**, 6, 29118.